MECHANISMS OF SEX DIFFERENCES IN RIGHT (-SIDED) HEART FAILURE: ROLE OF ANGIOGENESIS

by

Erica Seelemann

Submitted in partial fulfilment of the requirements
for the degree of Master of Science

at

Dalhousie University
Halifax, Nova Scotia
July 2022

TABLE OF CONTENTS

LIST OF TABLES

LIST OF FIGURES

ABSTRACT

Female sex is associated with better right ventricular (RV) adaptation and survival in patients with elevated RV afterload. Understanding the mechanisms responsible for sex differences in RV adaptation and development of right (-sided) heart failure (RHF) may uncover novel therapeutic targets for treatment of RHF patients. Therefore, this thesis investigated mechanisms of sex differences in RHF using Fischer CDF rats and the pulmonary artery banding (PAB) model.

Male and female Fischer CDF rats aged 5-7 weeks were subjected to pulmonary artery banding (PAB) or sham surgery; a subset was ovariectomized (OVX). Echocardiography and catheterization were performed at 1-, 2- and 4-weeks post-PAB to evaluate RV structure and function. Histological analyses were used to quantify sex differences in cardiomyocyte cross sectional area (CSA), and endothelial cell markers. A focused PCR array was performed to assess the expression of angiogenic genes in heart tissue. Primary right ventricular endothelial cells were isolated and effect of estradiol on angiogenic gene expression and network growth was assessed using RT-qPCR and Matrigel assay experiments, respectively.

At 1- and 2-weeks post-PAB, RV systolic pressure (RVSP) and RV hypertrophy (RVH) were significantly elevated in PAB rats compared to sham controls; however, no significant differences were observed between male and female rats. At 2-weeks post-PAB, male rats had a significant increase in the RV cardiomyocyte CSA (330 μm^2 vs 234 μm^2, $p<0.05$). RV internal diameter in diastole was also increased in male rats compared to female rats (3.33 mm vs 2.05 mm; $p<0.05$). Female rats had a higher cardiac index compared to male rats 2-weeks post-PAB. At 2-weeks post-PAB, the up-regulation of 24 angiogenic genes was observed in the RV of female rats compared to male rats.

In response to PAB, female Fischer CDF rats develop adaptive RV remodelling with better preserved RV function compared to maladaptive remodelling in male rats up to the 2-week timepoint. These sex differences are associated with a better RV angiogenic response in the female RV. Specific mechanisms for this effect are yet to be elucidated.

LIST OF ABBREVIATIONS USED

ACVS	Animal Care Committee of the Animal Care and Veterinary Services
BMPR2	Bone Morphogenetic Protein Receptor Type 2
CCAC	Canadian Council on Animal Care
CD	Collagenase Dispase
CHD	Congenital Heart Disease
CS	Charcoal Stripped
CSA	Cross Sectional Area
CTGF	Connective Tissue Growth Factor
DAB	3,3'-Diaminobenzidine
EBM2	Endothelial Basal Media 2
eNOS	Endothelial Nitric Oxide Synthase
EF	Ejection Fraction
EGM2-MV	Endothelial Growth Media2-MicroVascuature
ERα	Estrogen Receptor-α
ERβ	Estrogen Receptor-β
FAC	Fractional Area Change
FS	Fractional Shortening
FBS	Fetal Bovine Serum
GPER	G-Protein-Coupled Estrogen Receptor
H&E	Hematoxylin and Eosin Staining
HFpEF	Heart Failure with Preserved Ejection Fraction
HFrEF	Heart Failure with Reduced Ejection Fraction
HR	Heart Rate
HUVEC	Human Umbilical Vein Endothelial Cells
NO	Nitric Oxide
PA	Pulmonary Artery
PAB	Pulmonary Artery Banding
PH	Pulmonary Hypertension
PAH	Pulmonary Arterial Hypertension
LV	Left Ventricle

LV+S	Left Ventricle and Septum
RHF	Right Heart Failure
RV	Right Ventricle
RVAWd	Right Ventricular Anterior Wall Diastole
RVAWs	Right Ventricular Anterior Wall Systole
RVH	Right Ventricular Hypertrophy
RVIDd	Right Ventricular Internal Diameter Diastole
RVIDs	Right Ventricular Internal Diameter Systole
RVSP	Right Ventricular Systolic Pressure
SPHK1	Sphingosine Kinase 1
TAPSE	Tricuspid Annular Plane Systolic Excursion
TGFβ1	Transforming Growth Factor-β 1
TGFβ2	Transforming Growth Factor-β 2
TGFβ3	Transforming Growth Factor-β 3
TGFβR	Transforming Growth Factor-β Receptor
TOF	Tetralogy of Fallot
TR	Tricuspid Regurgitation
SRV	Systemic Right Ventricle
SD	Sprague-Dawley Rats
SuHx	Sugen Hypoxia
SV	Stroke Volume
VEGF	Vascular Endothelial Growth Factor
VTI	Velocity Time Integral
vWF	von Willebrand Factor

ACKNOWLEDGEMENTS

The work contained in this thesis would have been impossible without the support and mentorship of those around me. First and foremost, I would like to thank my supervisor, Dr. Ketul Chaudhary for trusting me to be his first master's student and introducing me to the world of cardiovascular research.

I would like to thank my committee members, Dr. Alex Quinn, Dr. Susan Howlett, Dr. Xianping Dong, and Dr. Yassine El-Hiani for their guidance and support. I would like to offer a special thanks to Dr. Howlett for access to the tools needed to conduct my echocardiography analysis and Dr. El-Hiani for access to the tools needed for my RT-qPCR experiments.

I would also like to thank Research Nova Scotia and Dalhousie University for funding my project and making my master's degree possible.

Beyond the lab, I would like to thank Dr. Mabel Ho, Dr. Marty Leonard, and the late Dr. Anne-Marie Ryan for their mentorship and encouragement. I value my professional development and the intrapersonal skills I have acquired the last two years as highly as my technical skills and results.

Finally, I would like to thank Kirishani Kesavan, Tony El-Rabahi, Michael Connolly, and Sheethal Panchakshari for their friendship during this chapter in my life. I appreciate your trust and understanding more than you know.

CHAPTER 1: INTRODUCTION

1.1 The Heart and the Right Ventricle

The heart is organized into four distinct chambers: the right and left atriums, and the right and left ventricles. Each side of the heart has a distinct function, as does each chamber. This thesis will focus on the right ventricle (RV), the chamber that forms the bottom right quadrant of the heart, and sex differences in its adaptations to an increase in RV afterload.

1.1.1 Right Ventricle Anatomy, Development, and Function

The RV is the dominant chamber of the heart during fetal development and operates in a relatively high pressure system (Cassin et al., 1964; Walker & Buttrick, 2013). This changes after birth when the RV becomes responsible for pumping deoxygenated blood to the lungs for oxygenation and the left ventricle (LV) begins pumping blood into systemic circulation. Post-birth, the RV undergoes reverse remodelling and becomes the thin-walled smaller chamber, whereas the LV becomes the dominant chamber and undergoes hypertrophy (Zelt et al., 2019). Pulmonary circulation is a low pressure and low resistance system due to the relatively high number of capillaries in the lungs. This vasculature creates a low afterload that the RV functions against after birth (Jain et al., 2022). Overall, the RV's unique function and anatomy make it an interesting focus of specific investigation unrelated to the LV.

1.1.2 Differences Between the Right and Left Ventricle

The LV is often viewed as the dominant side of the heart and the primary focus of research. This trend has led the RV to be considered the forgotten ventricle' of the heart (Tretter & Redington, 2018). It was believed for a long time that the findings from studies focused on the LV could be directly extrapolated to the RV; however, there are key differences between the LV and the RV that make the RV unique and warrant RV specific studies, including response to treatment (van Campen et al., 2016). Specifically, treatments designed for hypertension in the LV, like bisoprolol, a beta-blocker, are ineffective in patients with idiopathic pulmonary arterial hypertension (PAH) (Prisco et al., 2020; van Campen et al., 2016).

The RV and LV have different structures, function, and origin that make the RV worthy of independent investigation. Structurally, the RV has a lower mass and wall thickness compared to the LV (Walker & Buttrick, 2013). The LV is a prolate spheroid chamber compared to crescent shape of the RV (Ho & Nihoyannopoulos, 2006; Wang et al., 2019). In addition to the general differences in function and environment described above, there are important differences in contraction between the RV and the LV. Studies using Doppler and speckle tracking echocardiography have shown that systole in the RV is largely dependent on longitudinal fibers, unlike the LV (Chia et al., 2014). Further, detailed studies have examined regional RV function including basal, medial, and apex areas on both the septal and free walls (Chia et al., 2014; Kukulski et al., 2000). This work has shown that, likely due to the dependency on longitudinal fibers, the RV has higher long axis velocities than the LV and reduced circumferential shortening (Kukulski et al., 2000). The RV and LV also have different origins. During embryogenesis the RV, along with the primary outflow tract, develops from the pharyngeal mesoderm (Walker & Buttrick, 2013; Zaffran et al., 2004). The remainder of the heart is derived from the primary heart tube (Zaffran et al., 2004). The distinct structure, function, and origin of each ventricle make them, their pathology and their response to treatment unique (Piao et al., 2010; Voelkel et al., 2006). Importantly, treatments designed for the left side of the heart are ineffective on the right side and there are presently limited and largely ineffective treatments options for right (-sided) heart failure (RHF) (Konstam et al., 2018; van Campen et al., 2016). These differences warrant further examination into the function and structure of the RV independent from the LV.

1.1.3 Sex Differences in the Heart and the Right Ventricle

The male and female cardiovascular systems are notably different both anatomically and physiologically. Neither do they have congruent mechanisms for adapting to disease (Kawut et al., 2011). Much like the RV in relation to the LV, cardiovascular disease in females has been largely understudied compared to males because of the assumption that males and females develop pathophysiology and respond to treatments similarly. Unfortunately, this is untrue and has led to heart disease often going undiagnosed in sick

females (St. Pierre et al., 2022). The true extent of sex differences in heart disease, especially right heart disease, is largely unknown. Contributions from more recent works further demonstrated that standardized measurements in the RV vary between sexes. In a prospective study of men and women aged 45–84 years old who were free of clinical cardiovascular disease (the Multi-Ethnic Study of Atherosclerosis; MESA study), males were observed to have an approximately 8% higher RV mass than females; this observation was independent of age or race and adjusted for height and weight (Kawut et al., 2011). Interestingly, RV mass decreases in males and females as they age (Kawel-Boehm et al., 2015); however, the decrease in mass is proportionately greater in males (1 g/decade of life) compared to females (0.8 g/decade of life) when original body height and weight are considered (Kawut et al., 2011).

In the last decade, literature investigating physiology has focused on changes throughout the lifespan. Functionally, in children there is no significant difference in ejection fraction (EF) between sexes; however, after maturity, females have a higher EF and RV fractional area change (FAC) than males (Kawel-Boehm et al., 2015; Kawut et al., 2011; Lakatos et al., 2020; Sanz et al., 2019). These findings suggest that differences arise during sexual development and the mechanisms by which sex differences in RV physiology are developed during maturity are currently unknown. Understanding how these differences develop and the role of sex may allow for more effective and sex specific RV disease therapies, including therapies for RHF.

There are sex differences in the prevalence of RV pathology and RV function during pathology and stress. For example, PH has often been thought of as a ‘young women’s disease’ because of its prevalence in that demographic (Hester et al., 2019). Interestingly, while prevalent in young adult females, this group has better and less severe outcomes than males who develop PH. This phenomenon has been named “the Estrogen Paradox” (Hester et al., 2019).

1.2 Right Heart Failure

RHF is a condition in which the RV is unable to generate sufficient cardiac output (CO) to meet the body's demands (Thandavarayan et al., 2020). RHF can be defined as a clinical syndrome in which symptoms are caused by dysfunction that result in the RV having an impaired ability pump blood to the lungs (Mandras & Desai, 2022).

1.2.1 The Etiology of Right Heart Failure

Etiologies of RHF include pulmonary hypertension (PH), vascular disease, left heart diseases, congenital heart diseases, valvular disease, and ischemic heart disease (Walker & Buttrick, 2013). Regardless of origin, it is necessary to fundamentally understand RHF and the role of the RV in pathology to develop effective therapies.

1.2.1.1 Pulmonary Hypertension

PH is a prominent example of a condition that can lead to RHF. For a patient to be diagnosed with PH, resting mean pulmonary artery pressure must be greater than 25 mmHg (Hoeper et al., 2017). Increases in pulmonary arterial pressure cause increased RV afterload, ultimately leading to RHF and death. The increase in mean pulmonary artery pressure is induced by various causes (Hester et al., 2019), and PH can be divided into five groups based on the cause. These include:1) Group-1 PH: PAH; 2) Group-2 PH: caused by left heart disease; 3) Group-3 PH: caused by lung diseases; 4) Group-4 PH: chronic thromboembolic PH; and 5) Group-5 PH: unclear multifactorial mechanisms (Table 1) (Hester et al., 2019). Group-1 PH or PAH is a primary pathology and the most severe form of PH. Current treatments work by producing vasodilation of pulmonary arteries. The remaining PH groups are secondary forms of PH. Treatment options are focused on resolving the underlying cause of PH. For example, Group-2 PH may be treated indirectly by treating left heart failure (Sahay, 2019). Additionally, a recent Canadian study found that group-2 PH was the most common type of PH in Ontario (Wijeratne et al., 2018). Group-3 PH is caused by lung disease. It is caused by pathology creates a hypoxic condition in the pulmonary vasculature that ultimately leads to PH, the most common example chronic obstructive pulmonary disease (Poch & Mandel, 2021). Group-4 PH, chronic thromboembolic PH, develops in less than 5% of patients after a pulmonary embolism, but

it is often undiagnosed and can be fatal (Pengo et al., 2004; Poch & Mandel, 2021). Understanding the differences in the PH groups is necessary to understand their mechanisms and condition progressions.

Table 1: A summary of the PH group classifications, pathology source, and non-exhaustive list of common causes of each condition (Prins & Thenappan, 2016; Sahay, 2019).

PH group	Classification of PH	Pathology Source	Causes
1	Pulmonary arterial hypertension	Primary	Idiopathic (Prins & Thenappan, 2016)
			Hereditary (Prins & Thenappan, 2016)
2	Left heart disease	Secondary	Left heart failure
			Valvular disease (Prins & Thenappan, 2016; Sahay, 2019)
3	Lung disease	Secondary	Chronic obstructive pulmonary disease (Prins & Thenappan, 2016)
			Developmental lung disease (Prins & Thenappan, 2016)
4	Chronic thromboembolic	Secondary	Chronic thromboembolic pulmonary hypertension (Prins & Thenappan, 2016)
5	Unclear multifactorial mechanisms	Secondary	Metabolic disorders (Prins & Thenappan, 2016)
			Chronic renal failure (Prins & Thenappan, 2016)

1.2.1.2 Congenital Heart Disease

Congenital heart diseases (CHD) including Tetralogy of Fallot (TOF) and Eisenmenger's Syndrome can cause RHF. In these conditions the ventricular septum is abnormal or defective and blood is able to travel from the LV to the RV (Beghetti & Galiè, 2009). The increase in pulmonary blood flow causes sheer and circumferential stress in the vasculature, which leads to blood vessel damage and vasculature rarefaction. There is an increase in RV volume and pressure. Ultimately, these changes lead to RHF (Beghetti & Galiè, 2009).

Systemic right ventricle (SRV) is another common anatomical abnormality and it is present in 10-12% of all cases of CHD (Brida et al., 2018). This condition is notable by the transposition of the great arteries (Brida et al., 2018). This puts the stress of systemic circulation onto the RV. The SRV constitution includes unique fibromuscular architecture and an abnormal tricuspid valve (Brida et al., 2018). One distinct feature of SRV is that the RV loses its recognizable pointed shape and becomes rounder. It is worth mentioning that the anatomical abnormalities present in SRV lead to heart adaptations that are similar in patients with acquired heart diseases and increases in RV afterload, including PAH (Brida et al., 2018).

1.2.1.3 Valvular Diseases

Valvular diseases can also lead to RHF and are growing in prevalence as our population ages. Specifically, there has been an increase in degenerative valve diseases in the United States (Maganti et al., 2010). There are several forms of valvular diseases including valve regurgitation, stenosis, and prolapse. Directly impacting the RV, the tricuspid valve and pulmonary valve are susceptible to dysfunction. Tricuspid regurgitation (TR) occurs when the valve fails to seal the RV and this results in blood to returning to the right atrium. TR can occur as a primary condition through injury or age, but it more commonly presents as a secondary symptom or condition of another pathology (Antunes et al., 2017). Changes in RV pressure caused by PH and left-sided heart diseases can provoke secondary TR (Antunes et al., 2017). The pulmonary valve is largely understudied compared to the other valves in the heart (Pignatelli et al., 2017). Valve dysfunction including pulmonary valve regurgitation and pulmonary stenosis are both associated with right heart disease and can often be triggered by necessary surgical repairs to treat CHD (Kuang et al., 2020; Pignatelli et al., 2017). For example, surgical repair of TOF involves widening the stenotic pulmonary artery, which often causes valve regurgitation post-repair and, ultimately, increased load and dilation in the RV (Kuang et al., 2020).

1.2.1.4 Remodelling Differences in Pressure and Volume Overload

Pressure and volume overload lead to differences in ventricular remodelling. Increase in pulmonary artery pressure, as is the case in PH, cause increases in afterload, which is the

pressure the RV is opposing during contraction (Pitoulis & Terracciano, 2020; Sanz et al., 2019). The ventricular wall thickens, cardiomyocytes hypertrophy, and the RV hypertrophies to adapt to the increase in pressure (Grossman & Paulus, 2013; Pitoulis & Terracciano, 2020; Sanz et al., 2019). The chamber's hypertrophy is associated with an angiogenic response that is needed to adequately supply the hypertrophied tissue with oxygen and nutrients (Sanz et al., 2019). Volume overload can be caused by dysfunctional heart valves, specifically regurgitation, or CHD structural anomalies that increase preload (Pitoulis & Terracciano, 2020). Volume overload occurs when blood re-enters the RV post-ejection. This causes in an overall increase in blood volume during diastole that the heart is ill-equipped to support (Pitoulis & Terracciano, 2020). In contrast to the ventricle dilation and thickening seen in pressure overload, this leads to ventricular chamber dilation and no change or thinning of the ventricular wall, (Carabello, 2002; Pitoulis & Terracciano, 2020). Importantly, the atypical displaced volume in RV volume overload often causes LV dysfunction as well (Sanz et al., 2019). Distinguishing the types of overloads and their morphology from each other to better understand model and natural disease progressions of RHF.

1.2.2 The Role of Right Ventricular Function in Patient Survival

RV function is a critical determinant of the severity of functional impairment and one of the strongest indicators for survival of patients with PH, heart failure with preserved ejection fraction (HFpEF) and with heart failure with reduced ejection fraction (HFrEF) (van de Veerdonk et al., 2011; Walker & Buttrick, 2013). RV dysfunction is common in patients affected by left-sided heart failure. Around 20-50% of patients with (HFpEF) and 50-75% of patients with HFrEF have been reported to have RV dysfunction (Burke et al., 2014). Stable RV function, measured as RVEF, is a strong predictor of survival in patients with PAH. Preserving RV function is necessary for survival, but unfortunately there are no targeted therapies that have been designed specifically for the failing RV and current treatments, including digoxin, 7asix, and intravenous inotropes, are largely ineffective (Piao et al., 2010).

1.2.3 Pathophysiology and Mechanisms of Right Ventricular Remodelling

Chronic RV pressure overload leads to RV remodelling, a heterogeneous process that has two potential outcomes. Despite similar increases in RV afterload, individuals exhibit either adaptive RV remodelling or maladaptive RV remodelling. Adaptive RV remodelling is characterized by preserved RV function (maintained CO, EF, and exercise capacity; a compensated RV) and structure (minimal RV dilation and fibrosis). In contrast, maladaptive RV remodelling is characterized by a reduced cardiac function (decreased CO, EF and exercise capacity; a decompensated RV) and adverse structural remodelling (increased RV dilation and fibrosis) hypertrophy, and ultimately death (Frump et al., 2018). PH is an excellent example of pathology with sex differences in condition prevalence, outcomes, and structural remodelling.

Currently, the exact mechanism(s) responsible for differential RV adaptation and development of RHF are unknown, including the role that sex may play. However, recent work has indicated that metabolic changes (Piao et al., 2010), fibrosis, inflammation (Zelt et al., 2019) and angiogenesis (Frump et al., 2018) or lack of it, play an important role in maladaptive RV remodelling and development of RHF.

1.2.3.1 The Role of Angiogenesis in Right Heart Failure

Angiogenesis is the growth of new blood vessels via sprouting from existing vasculature and it is necessary to maintain or increase vascular density in different pathologies (Gogiraju et al., 2019; Goumans et al., 2009; Ribatti, 2013). The increase is necessary to adequately perfuse the surrounding tissue (Gogiraju et al., 2019). Angiogenesis is regulated by several different signaling pathways, including PI3K/Akt and MAPK (Zhang et al., 2022). Activation of P13K /Akt leads to the upregulation of endothelial nitric oxide synthase (eNOS), which supports the production of nitric oxide (NO) and ultimately angiogenesis (Zhang et al., 2022) (Figure 1). Another critically important factor in angiogenesis and vascular density is vascular endothelial growth factor (VEGF) (Giordano et al., 2001; Yancopoulos et al., 2000). Researchers have shown that deletion of the VEGF gene in mice led to impaired micro-vasculature and impaired contractile function (Giordano et al., 2001). Moreover, VEGF supplementation can delay indicators of

maladaptive remodelling in rabbits subjected to aortic banding (Friehs et al., 2006; Gogiraju et al., 2019). VEGF initiates blood vessel growth by increasing endothelial cell proliferation in vascular tissue (Gogiraju et al., 2019; Yancopoulos et al., 2000). For more in-depth information on angiogenic signaling in cardiovascular disease please refer to the review by Gogiraju et al (Gogiraju et al., 2019; Yancopoulos et al., 2000)

Clinical and pre-clinical studies have demonstrated that adaptive RV remodelling is accompanied by angiogenesis, whereas maladaptive remodelling is associated with an inadequate angiogenic response (Potus et al., 2015; Suen et al., 2019). Specifically, Potus et al., demonstrated that patients with decompensated RV failure had reduced vascular density compared to healthy patients and patients with compensated (right ventricular hypertrophy) RVH (2015). They demonstrated that the decompensatory response was associated with reduced microRNA-126 levels. MicroRNA-126 is involved in the VEGF angiogenic pathway (Potus et al., 2015). Suen et al. utilized the Sugen hypoxia (SuHx) model of PH, discussed later in this thesis, and studied RV remodeling in Fischer CDF and Sprague-Dawley (SD) rats (Suen et al., 2019). They showed that Fischer CDF rats had much poorer survival outcomes than SD rats that was associated with reduced angiogenesis and the down-regulation known angiogenic genes (Suen et al., 2019). In summary, current clinical and pre-clinical data indicate that an adequate angiogenic response during RV remodelling may be necessary for RV adaptation and to prevent development of RHF. An effective adaptation includes an increase in angiogenesis that maintains the proportion of capillaries to cardiomyocyte area (Frump et al., 2018). In other words, cardiomyocyte hypertrophy needs to be accompanied by an increase in blood vessels for the cardiomyocytes to remain sufficiently fueled (Figure 2).

Given the literature examining the role of angiogenesis in RV adaptations to increased afterload, it is important to examine genes possibly involved. Of note, Sphingosine Kinase 1 (SPHK1), Transforming Growth Factor-β (TGFβ), and Connective Tissue Growth Factor (CTGF) (also known as Cellular Communication Network Factor 2) are three known pro-angiogenic genes investigated in this thesis.

Research has shown that SPHK1 is active in cardiovascular development and function (Jozefczuk et al., 2020). SPKH1 contributes directly to the production of Sphingosine-1-phosphate (S1P), which binds to the Sphingosine-1-phosphate (S1P1) receptor (Figure 1). SIP has also been associated with strengthening the endothelial cell barrier and supporting cell regulation (Xiong & Hla, 2014). Previous work has further demonstrated that SPHK1 is also pro-angiogenic in human umbilical vein endothelial cells (HUVEC) and bovine aortic endothelial cells (Sukocheva et al., 2015). The effects of S1P both intracellularly and through S1P1 are complex and multi-faceted to ensure vascular homeostasis (Siedlinski et al., 2017). Different S1P receptors have different effects on different systems (Means & Brown, 2008). S1P1 is the most abundant S1P receptor in cardiac endothelial cells, and pro-angiogenic in nature (Means & Brown, 2008). Research has also demonstrated that SPHK1 knockout mice show delayed wound closure due to a lack of angiogenesis (Aoki et al., 2019). Overall, it is largely accepted that SPHK1 is pro-angiogenic in nature. Further examination into the role of SPHK1 in other endothelial cells, including cardiac endothelial cells is warranted.

The cytokine family TGFβ is complex. It has multiple roles in regulating endothelial cell pathways that have yet to be fully understood (Goumans et al., 2009). It can both inhibit as well as promote angiogenesis (Goumans et al., 2009). Endothelial cells are regulated by TGFβ through activin receptor-like kinases (ALK) ALK1 and ALK5 (Goumans et al., 2009). ALK5 inhibits angiogenesis via Smad 2 and 3 whereas ALK1 is pro-angiogenic and promotes the phosphorylation of Smad 1 and 5. Phosphorylation of Smad 1 and 5 allows them to complex with Smad4 and translocate into the nucleus (Figure 1). Interestingly, ALK1 and ALK5 physically interact with each other and a functional ALK5 is necessary for optimal ALK1 activity (Goumans et al., 2003, 2009). TGFβ's key role in cardiovascular physiology and the development and maintenance of vasculature was partially recognized when researchers discovered that mouse models deficient in TGFβ receptors were embryonic lethal due to angiogenic defects (Goumans et al., 2003, 2009; ten Dijke & Arthur, 2007). Given the diverse role of the TGFβ family, we investigated the role of TGFβ1, TGFβ2, TGFβ3, and TGFB receptor (TGFβR) in this thesis.

The involvement of CTGF has been shown in a variety of cellular functions, including those related to tissue vascularization. Recently, research has shown that endothelial cells are a major source of CTGF in the retina and mice with reduced CTFG expression are likely to have reduced vascularization in the retina (Moon et al., 2020). Researchers have also shown that bone marrow stromal cells upregulate CTGF in patients with heart failure (Minullina et al., 2014). Other work has shown that CTGF is upregulated via Norepinephrine and that CTGF in a complex with VEGF may support endothelial cell tube formation (Lai et al., 2013). These findings warrant further investigation of CTGF's involvement in vascular development.

Overall, the roles that SPHK1, TGFβ, and CTGF play in endothelial cell regulation, blood vessel growth and maturation, and healthy tissue vascularization, make them strong candidate genes worth examining in the context of cardiac endothelial cell growth and angiogenesis.

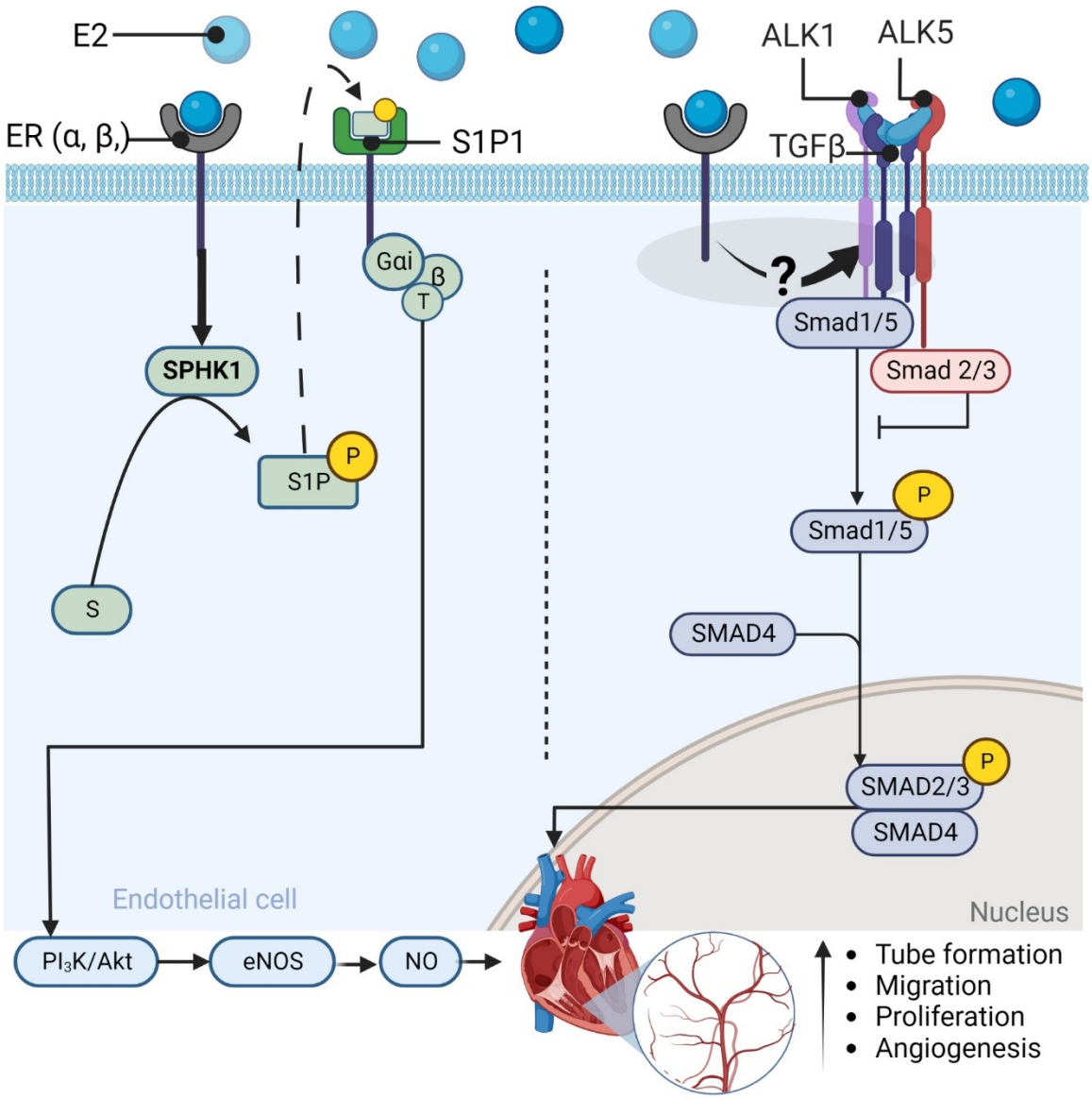

Figure 1: SPHK1 and TGFβ proposed mechanism of action for regulating angiogenesis in endothelial cells based on work by Sukocheva et al., (2015) and Goumans et al.'s review (2009). E2 promotes the phosphorylation of S to S1P, which attaches to the S1P1 recepto and triggers activation of the $P1_3K$/Akt angiogenic pathway. TGFβ in conjunction wth ALK1 and ALK5 triggers the activation of Smad 1 and 5. The phosphorylated Smad1/5 creates a complex with Smad4 to enter the cell nucleus. Made with BioRender

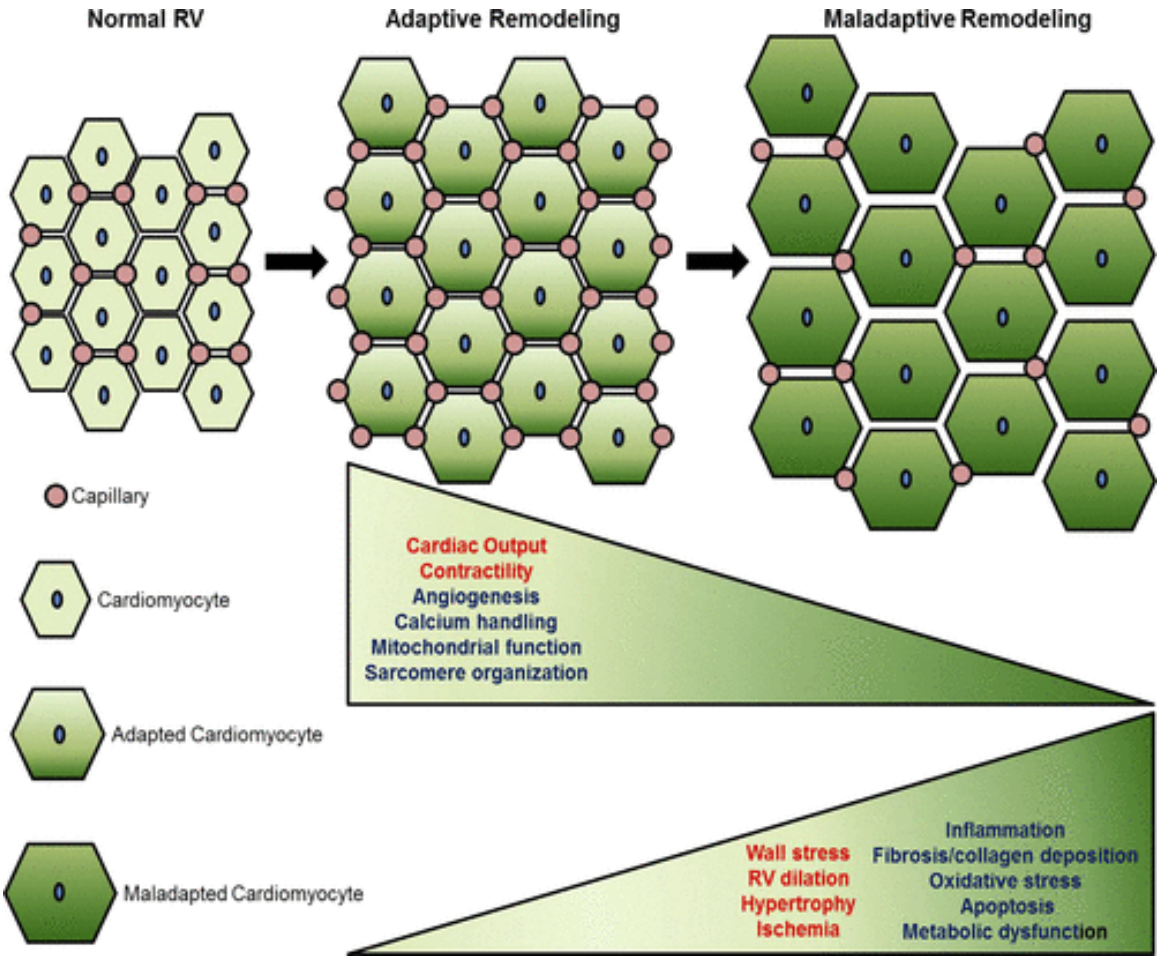

Figure 2: A representation of how the proportion of capillaries to cardiomyocyte area must remain consistent during pathology for the heart to adaptively remodel. Disproportionate growth is associated with reduced cardiac output and contractility; it is positively associated with increase wall stress, RV dilation, hypertrophy, and ischemia. This image was taken with permission from Frump et al. (2018). Copyright © 2022 the American Physiological Society

1.2.3.2 Metabolic Changes in Right Heart Failure

RHF can develop as a consequence of metabolic changes in the RV. Research has shown that patients with PAH, and more specifically RVH, uptake an excessive amount of glucose and are energy deficient. As glucose becomes the primary energy source, there is a shift away from its oxidation to glycolysis (Zelt et al., 2019). Importantly, glycolysis is not nearly as effective as glycose oxidation regarding ATP yield. The cardiovascular systems in patients who are suffering from an ATP deficiency that may present itself as contraction impairments that can lead to the development of RHF (Piao et al., 2010; Zelt et al., 2019). Overall, the literature suggests that metabolic pathways have a critical role in RV remodelling.

1.2.3.3 Fibrosis and Inflammation Changes in Right Heart Failure

Two other important factors involved in RV adaptation are fibrosis and inflammation. Myocardial fibrosis is the result of modifying the extracellular matrix between cardiomyocytes with collagen. The material change to the RV further disrupts its function. An increase in stiffness limits contractility and can ultimately expedite the development of RHF (Heymans et al., 2015). Myocardial fibrosis can be described as “replacement” or “reactive”. The former is in response to acute injury and the latter is in response to chronic overload, as is the case in RHF (Schimmel et al., 2022). Additionally, the replacement can be interstitial or perivascular. While not mutually exclusive, interstitial fibrosis is seen in models of PH and perivascular remodelling is more prevalent in the pulmonary artery banding (PAB) model, which creates an immediate increase in afterload in the RV (Zelt et al., 2019). Overall, fibrosis is detrimental to the RV and can act as a catalyst for RHF.

Another potentially impactful symptom in the development of RHF is inflammation. It is well accepted that excess inflammation is a detriment to RV contractility and other measures of function (Zelt et al., 2019). Initial inflammatory responses can support vascular remodelling and angiogenesis. However, in chronic conditions, like PAH, pro-inflammatory markers are found in excess in the tissue with increasing infiltration, suggesting a link between inflammation and pathology (Sun et al., 2017).

Interestingly, it has been shown that Fischer CDF rats are more prone to develop RHF than Sprague-Dawley rats and that Fischer CDF rats also have a reduction in the expression of genes linked to the development of natural killer cells. It has been demonstrated that natural killer cells support angiogenesis (Suen et al., 2019). It is necessary to further investigate the role of acute and chronic inflammation in RHF and the involvement of specific pro-inflammatory markers.

1.3 Rat Models of Right Heart Failure Research

Animal models, especially rats, have been one of the primary models of investigating the mechanisms of RHF. With rats, there are three common methodologies that can directly induce RHF or lead to RHF by mimicking the natural progression of PH. These are SuHx, monocrotaline (MCT), and PAB. The SuHx model of PH involves a single subcutaneous injection of sugen followed by a 3 week period of chronic hypoxia exposure (Jiang et al., 2016; Suen et al., 2019). The combination causes rats to develop PAH, characterized by a significant increase in right ventricular systolic pressure (RVSP) and RVH (Suen et al., 2019). SuHx is a useful model of PAH because it mimics natural PH progression. It disrupts endothelial cells and is the model that best recapitulates the hallmark feature of human PAH , the plexiform-like vascular lesions (Evgenov et al., 2013). However, a limitation of this method is that the sugen injections can have a systemic effect on the subject that confound more pointed investigations, like the mechanisms of RHF. MCT is an alkaloid that, post a single injection of 60-100mg/kg, leads to the development of PH in rats over a period of weeks (Evgenov et al., 2013). Similar to SuHx, MCT disrupts endothelial cells. Some benefits of the MCT model are that it is relatively low cost, effort, and easily reproducible (Gomez-Arroyo et al., 2012). The model is limited by the immediate injury that the MCT injections cause, as well as confounds from airway damage and myocarditis (Evgenov et al., 2013). Finally, and as mentioned briefly, PAB is surgical method that involves constricting the pulmonary artery (PA) (Evgenov et al., 2013). This immediately increases afterload in the in RV and causes the heart to adapt or maladapt in response to the increase in pressure. This method is useful for examining RHF because the intervention is very specific and targets the RV. However, the targeted nature of this intervention also means that it is unreflective of natural cardiac pathologies and requires complex surgical

skills (Evgenov et al., 2013). The SuHx and MCT methods of PH are more gradual than PAB and mimic natural PH pathology that can ultimately lead to RHF. Unfortunately, their systemic nature creates potential confounds when specifically investigating the physiology of the RV during RHF. The chemical nature of SuHx and MCT are also potentially confounding in experiments examining the role of sex hormones.

Previous work linked to our lab has demonstrated that the Fischer CDF rat strain is more susceptible to RHF than SD rats using the SuHx model (Suen et al., 2019). Specifically, Suen et al. explain that in SUHx model both SD and Fischer rats develop similar PH and lung vascular remodelling. Despite similar pulmonary disease, RV remodelling was different between rat strains, including significant differences in vascular density, and that difference was associated with observed differential survival where SD rats had much better survival outcomes than Fischer CDF rats (2019). The conclusion that Fischer CDF rats may be susceptible to RHF. Therefore, studied in this thesis used the Fischer CDF rat PAB model to study RHF.

1.4 Sex Differences in Right Ventricular Adaptation and Right Heart Failure

1.4.1 Sex Differences in Human Patients

Prevalence of diseases that lead to right heart diseases, such as PAH, have markedly different prognosis dependent on sex. Group-1 PH, PAH, is irreversible, unlike PH (Hoeper et al., 2017). Interestingly, PAH registries from around the world suggest that females make 65%-80% of PAH patients (Hester et al., 2019). However, males have worse survival outcomes for PAH despite lower incidence than females (Foderaro & Ventetuolo, 2016; McGoon & Miller, 2012; van de Veerdonk et al., 2016; Yoo, 2018). Additionally, researchers have linked estradiol and lower levels of androgens to the protective effects present in females (van de Veerdonk et al., 2016). However, a recent review suggests that the current literature is not comprehensive enough to establish concrete relationships between the role of androgens and heart disease (Lewis & Houstis, 2019). Understanding the mechanisms responsible for these sex differences in right heart disease may provide valuable information necessary to develop targeted therapies.

1.4.2 Sex Differences in Animal Models

The effects that androgens have on the female sex have yet to be conclusively determined. Androgens may be a critical component to understanding causes and protections of cardiovascular disease between sexes. Hemnes et al. investigated the effect of testosterone on mice that underwent PAB or were castrated (Hemnes et al., 2012). Their study produced three major findings about the effects of testosterone. Firstly, they demonstrated that testosterone supplementation had a minimal effect on RV function. *In vivo* measurements suggested that there were no significant effects of testosterone on RV systolic pressure and diastolic pressure (Hemnes et al., 2012). Secondly, in response to an increase in afterload, testosterone increased RV fibrosis and myocyte hypertrophy (Hemnes et al., 2012). In the PAB group, RV hypertrophy and fibrosis was reduced in castrated the mice. Moreover, testosterone supplementation caused hypertrophy and fibrosis to increase. Thirdly, animals that underwent PAB in the absence of testosterone had improved survival outcomes (Hemnes et al., 2012). These findings suggest that in stressed conditions, specifically PAH, testosterone may contribute to maladaptive remodelling. It is also noteworthy that high levels of estrogen and low levels of testosterone are negatively correlated with cardiovascular disease in senior males (Ventetuolo et al., 2011). Overall, the literature suggests that testosterone may be detrimental to cardiovascular health in pathology.

Estrogen is pro-angiogenic in nature (Arnal et al., 2010; Garvin et al., 2005; Losordo & Isner, 2001; Sukocheva et al., 2015). This is true systematically, and in disease as well as healthy state. For example, estrogen upregulates angiogenesis in breast cancer tumors (Garvin et al., 2005). Common treatments involve estrogen receptor antagonists, including tamoxifen, to prevent angiogenesis via the VEGF pathway and starve the cancer (Garvin et al., 2005). It has also been shown that estrogen upregulates angiogenesis in cultures of HUVEC (Sukocheva et al., 2015). Additionally, in a study conducted by Liu et al., researchers discovered that estrogen supports the preservation of mitochondrial content and oxidative capacity (A. Liu et al., 2017). In the case of endothelial cell injury, estrogen is associated with recovery (Trenti et al., 2018).

Beyond estradiol's role in angiogenesis systemically, it also has angiogenic effects specifically in the RV that are modulated by estrogen receptors. There are 3 estradiol receptors namely estrogen receptor-α (ERα), estrogen receptor-β (ERβ) and G-protein-coupled estrogen receptor (GPER), all have been shown to be expressed in the RV (Frump et al., 2015). Frump et al. demonstrated that ERα expression is higher in female RV compared to male RV and the expression decreases in female RV in response to SuHx (Frump et al., 2015). Interestingly, estradiol up-regulates ERα expression in the RV. On the contrary, ERβ expression in lower in female RV compared to males but it is not affected by SuHx or estradiol treatment. Similar to ERα, GPER expression is higher in female RV and it is down-regulated by SuHx; however, estradiol treatment does not affect GPER expression in the RV (Frump et al., 2015). ERα density was also negatively associated with RVSP and RVH, which suggests that ERα is protective against maladaptive remodelling (Frump et al., 2015). Interestingly, protective effects were replicated, albeit less profoundly, when SuHx OVX rats were treated with an ERβ agonist suggesting that both receptors are cardioprotective against RV maladaptation (Frump et al., 2015). Recent work has demonstrated that 17β-estradiol may activate ERα which modulates the bone morphogenetic protein receptor type 2 (BMPR2) promoter to regulate and increase apelin, which is cardioprotective in nature (Frump et al., 2021). Progesterone receptors are also expressed in the heart and have been suggested to play a role in sex-specific maturation of metabolic programs and maturation of contractile function (Sim et al., 2021). Taken together, is it well established that estrogen has cardioprotective effects and, estrogen and progesterone receptors are expressed in the RV. However, the precise mechanisms of sex differences in RV angiogenesis remain unknown and need to be elucidated.

1.5 Objectives and Hypothesis

The literature on RV physiology recognizes the sex differences described above. However, the mechanism(s) by which sex differences in RV's pathophysiology are developed during disease are currently unknown. Understanding how these differences develop may allow for more effective and targeted RV disease therapies.

1.5.1 Objectives

The overall objective of this thesis is to describe sex differences in the development of RHF in Fischer CDF rats in a PAB model and to further investigate the mechanism(s) underlying these differences. Specifically, the objectives are:

1. To compare structural and functional differences in the RV of male and female Fischer CDF rats in a PAB model of RHF.
2. To elucidate the possible mechanisms responsible for observed sex differences.

1.5.2 Hypothesis

Given the literature demonstrating the pro-angiogenic nature of estradiol, critical role of angiogenesis in preventing development of RHF, and sex differences in RHF, we hypothesized that the ability of females to better adapt to elevated RV afterload, compared to males, is supported by a stronger angiogenic response in the female RV.

CHAPTER 2: METHODOLOGY

Contributions: PAB surgery, hemodynamic measurements, and echocardiography were completed by Dr. Ketul Chaudhary and analyzed by Erica Seelemann. RT-qPCR for tissue samples was performed by Sheethal Panchakshari. Primary male RV endothelial cells (RVEC) used in this thesis were originally isolated by Kirishani Kesavan and the original cell isolation protocol has been further optimized by Erica Seelemann. Please note: Erica has successfully isolated male and female RVECs and the female RVECs are currently being used by other lab members. All other work was completed by Erica Seelemann.

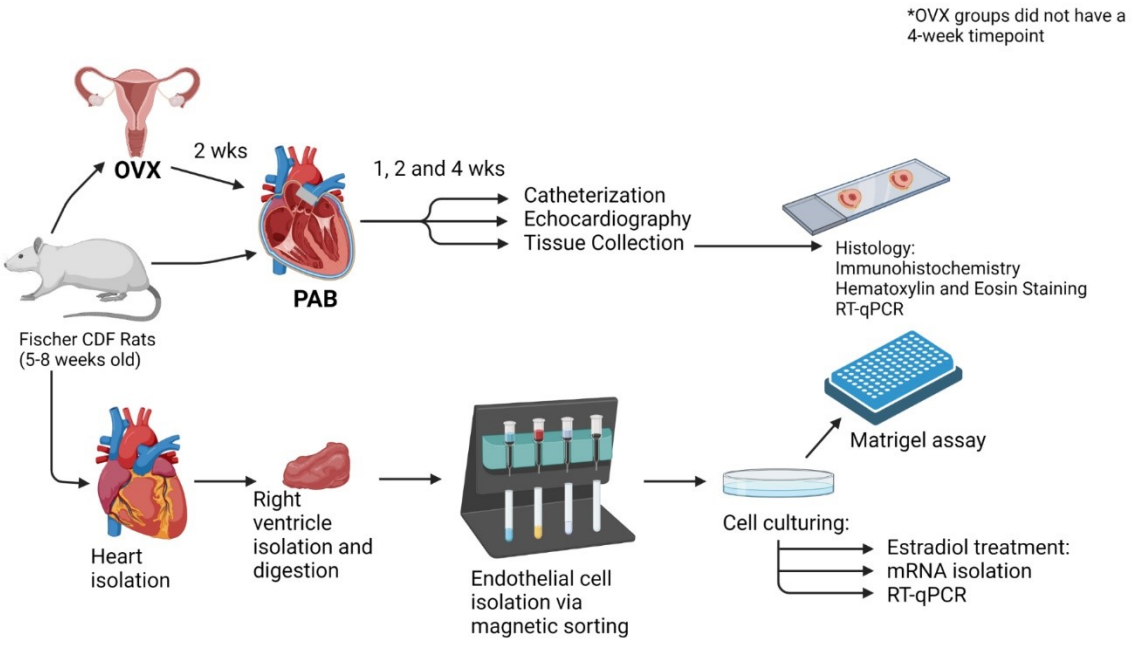

Figure 3**:** Experimental overview for methodologies used in this thesis. Adult male Fischer CDF rats were subjected to pulmonary artery banding (PAB). At 1-, 2-, or 4-weeks post-PAB, echocardiography was performed. At the animal's end point catheterization and tissue collection occurred; the latter was used for histological analyses. Ovariectomized females were examined in a different experimental cohort. They were ovariectomized two weeks pre-PAB. Independently, heart isolations were performed on naïve male Fischer CDF rats. From these samples, endothelial cells were isolated and used for ex vivo cell culturing experiments. Image created using BioRender.

3.2 Animal Care and Handling

All animal procedures were approved by the Animal Care Committee of the Animal Care and Veterinary Services (ACVS) of the University of Ottawa or University Committee on Laboratory Animals (UCLA) of Dalhousie University and were in accordance with the Canadian Council on Animal Care (CCAC) guidelines. Adult Fischer CDF rats, aged 5-8, were obtained from Charles River Laboratory (Montreal, QC, Canada) and were given at least one week to acclimatize before any procedure. OVX female Fischer CDF rats were purchased from Charles River Laboratory (Montreal, QC, Canada). Throughout the experiments, all rats were maintained on a light-dark (12 hours/12 hours) cycle and had access to food and water ad libitum.

2.2 Pulmonary Artery Banding Surgery

Rats were anesthetized in an induction chamber using isoflurane inhalation (5% isoflurane, 1 L/min O_2). Immediately post-induction, tracheal intubation was performed using a 14 G blunt angiocath that was used to ventilate the rats and maintain anesthesia throughout the entire procedure (tidal volume: 1.0 mL; respiratory rate: 100 breaths/min; 2% isoflurane, 1 L/min O_2). After confirming surgical plane anesthesia and successful mechanical ventilation, a left thoracotomy was performed in the third intercostal space followed by the section of the intercostal muscles under sterile conditions. The pleura was opened and the left lung was mobilized. The pulmonary trunk was located and a 4-0 silk thread was positioned under the PA immediately distal to the pulmonary outflow tract. An 18-gauge needle was held on top of and in parallel with the PA. The suture was tightened around the artery and needle, then the needle was removed rapidly. The constriction limited the size of the artery opening to the outer diameter of the needle (1.27 mm). Needle gauge was chosen to create an approximately 70% restriction to PA size.

The chest was closed with 2-0 VICRYL loop for intercostal spaces. Muscle and skin layers were closed with 4-0 polypropylene sutures. Rats were disconnected from the ventilator and, upon confirmation of spontaneous respiration, extubated and placed in a recovery cage. Rats received buprenorphine (0.05 mg/kg; 1 hr before and 6, 24 and 48 hr post-surgery) and carprofen (2.5 mg/kg; 1 hr before and 24 and 48 hr post-surgery) for pain

management. In addition, topical bupivacaine was applied to the wound area upon closure, at 6 and 24 hr post-surgery. Male and female rats in the control group were subjected to a sham surgery. For the sham surgery, a thoracotomy was performed under anesthesia. The PA was separated and a suture was placed under the PA; however, the suture was removed without vessel occlusion and the chest was closed as described above.

2.3 Estradiol Treatment

Sex hormone replacement was performed using continuous slow-release pellets (17β-estradiol: 0.5 mg pellet, s.c., 60-day release; Innovative research America, USA). Immediately prior to PAB/sham surgery, rats were randomized to receive estradiol or placebo pellets. Rats were anaesthetized by isoflurane inhalation and slow-release pellets were implanted subcutaneously on the dorsal side at the base of the neck. Following the implantation of a pellet, the animals were subjected to PAB or sham procedure as described earlier. Topical bupivacaine was applied immediately after wound closure and twice daily for one day post-surgery. Buprenorphine (s.c., 0.03mg/kg) was administered 1 hr prior to surgery and once daily for two days post-surgery.

2.4 Echocardiography

Rats were anesthetized by isoflurane inhalation (5% isoflurane, 1 L/min O_2) using an induction chamber. Rats were then removed from the chamber and placed on a heated plate (37 °C) with their nose placed into a nose cone supplied with isoflurane (2% isoflurane, 1 L/min O_2). The eyes were treated with a petroleum-based ophthalmic ointment and the chest was shaved and cleaned with distilled water. Ultrasound gel was applied on the chest of the anesthetized rat and echocardiographic images were acquired. Using a parasternal long axis view, the aorta was located and the probe was rotated clockwise to locate the PA. B-mode images were acquired for PA diameter and pulse wave Doppler mode was used to measure PA velocity time integral (VTI). Using PA diameter and PA VTI, stroke volume (SV) (Equation 1) and CO (Equation 2) were calculated. Using PA diameter, we calculated the circle area of the PA and gauge used to determine what percent of the PA was restricted by PAB (Equation 3). Parasternal short axis view was used to acquire M-mode images to obtain RV free wall thickness, diastolic RV internal diameter (RVIDd), diastolic left

ventricular internal diameter (LVIDd), fractional shortening (FS), and HR. Apical four chamber view was used to assess the RV chamber area during diastole and systole to measure FAC and assess the tricuspid annular plane systolic excursion (TAPSE). Following echocardiography, rats were placed in a recovery cage, and, following complete recovery, transferred to a housing cage.

Equation 1: $SV = 3.14\ (\frac{PA\ Diameter}{2})^2 \times \text{VTI}$

Equation 2: $CO = SV \times HR$

Equation 3: $PA\ \%\ occlusion = \frac{\pi(\frac{1.29mm}{2})^2)}{(\pi(\frac{PA\ diameter}{2})^2} \times 100 - 100\ \times (-1)$

2.5 Catheterization

RVSP was measured using high-fidelity pressure catheters (Transonic-Scisense Inc., ON, Canada) at the end of the study (1-, 2- or 4-week post-PAB). For RV catheterization, rats were anaesthetized by an intraperitoneal injection of xylazine (7 mg/kg) and ketamine (35 mg/kg). The pressure catheter was inserted into the right jugular vein and advanced through the superior vena cava and right atrium into the RV. Hemodynamic parameters were recorded and analyzed using the LabScribe3 software (iWorx, Dover, NH, USA). The operators acquiring the RVSP data were blinded to the treatment condition.

2.6 Heart Isolation and Preparation of Tissue Paraffin Blocks

Immediately following catheterization, the abdominal cavity was opened and the rats were sacrificed via exsanguination by dissecting the inferior vena-cava. The open abdominal cavity was expanded and the diaphragm was cut to expose the heart and lungs. Once exposed, the thoracic cavity was further expanded so the aortic arch could be seen. Surgical scissors were carefully slid behind the heart to separate any remaining fiber attachments and used to extricate the heart by cutting the aortic arch. The ventricles were dissected from the atria, the aorta, and the pulmonary trunk. The RV was separated from the LV and septum (LV+S) and RV hypertrophy was calculated by measuring the ratio of RV weight to LV+S weight (RV/LV+S, Fulton index). The RV and LV+S were placed in 4% paraformaldehyde for 48 hr followed by a 24 hr Phosphate-Buffered Saline Solution (PBS)

wash, and then preserved in 70% ethanol until paraffin embedding (Leica EG1160 embedding station, Leica Biosystems Inc, ON, Canada).

2.7 Heart Tissue Sectioning and Histology

To prepare tissue for histological experiments, tissue blocks were sectioned (5 µm thickness) with a microtome (Leica Microsystems, Concord, ON, Canada), placed onto poly L lysine-coated slides, dried at 37°C for 16 hr, and then dewaxed and rehydrated through graded alcohols. Briefly, sections were submerged in xylene three times for 5 min each, followed by two 2 min incubations in 100% ethanol. Next, sections were submerged for 1 min in 90% ethanol and then 1 min in 70% ethanol. Finally, sections were placed in double distilled water for 5 min. After rehydration slides were stained using immunohistochemistry or hematoxylin and eosin (H&E) as per manufacturer's instructions. Slides were dehydrated and then sealed using Cytoseal media and a coverslip. Slides were left overnight to fully dry before microscopy.

2.7.1 Hematoxylin and Eosin Staining

To assess cardiomyocyte cross sectional area (CSA), we performed H&E staining on 5 µm sections of heart samples collected from PAB rats. Sections were stained with the H&E Stain Kit (CAT# ab245880, Abcam, MA, USA) as per manufacturer's protocol. Briefly, slides were deparaffinized and then incubated in 100 µL of Hematoxylin, Mayer's (Lillie's Modification) for 5 min. Slides were rinsed with two changes of distilled water and then incubated in 100 µL per section of the Bluing Reagent for 10-15 sec. Slides were rinsed in two changes of distilled water and then dipped in absolute alcohol. Excess alcohol was blotted off with a KimTech wipe before 100 µL of Eosin Y Solution (Modified Alcoholic) was added to each section and allowed to incubate for 2-3 min. Slides were rinsed in absolute alcohol and transferred to 70% ethanol for further dehydration and mounting.

Images were taken using a LMI-3000Series Routine Inverted Microscope (LAXCO, WA, USA) at 20X magnification with a SeBaCam Digital Camera (PN:SeBACam100; Laxco, WA, USA) and SeBAView software (Laxco, WA, USA). Using ImageJ's (National Institutes of Health, MA, USA) Freehand Selection tool, the perimeters of 20 cells in 3-5

images per ventricle were traced and cardiomyocyte CSA was calculated. Only cardiomyocytes cut cross-sectionally were included in this analysis. Longitudinal sections and those with unclear orientations were omitted. CSA was averaged for each section and averages for each experimental condition were further averaged.

2.7.2 Immunohistochemistry

To investigate the density of EC, we performed IHC for EC-specific marker von Willebrand Factor (vWF) on the heart sections obtained from rats subjected to PAB or sham surgery. Antigen unmasking solution was made using 500 mL of distilled water and 4.9 mL of Citric Acid Based Antigen Unmasking Solution (CAT# H-3300-250 Vector Laboratories, CA, USA). It was prewarmed in the microwave for 3 min and then deparaffinized slides were submerged and microwaved on high for 12 min. Slides were left to cool at room temperature for an additional 15 min. Then, they were rinsed in a tap water bath and washed in PBS buffer for 5 min.

Rabbit specific HRP/DAB (ABC) Detection kit (CAT# ab64261Abcam, MA, USA) was used for IHC. First, slides were incubated with hydrogen peroxide for 10 min and washed twice with PBS with Tween^{TM} 20 (PBS-T) for 5 min each. Next, non-specific staining was blocked using protein block for 20 min and then washed once with PBS-T for 5 min. Following the washes, the rabbit polyclonal antibody against vWF (CAT# ab6994, Abcam, MA, USA) was used at a 1:2000 concentration with 2% BSA-PBS and incubated for 1 hr at room temperature. Following incubation, slides were washed with PBS-T four times for five minutes each and then incubated with Biotinylated Goat Anti-Polyvalent at room temperature for 15 minutes. Slides were washed with PBS-T four times for 5 minutes each time. Sections were incubated with Streptavidin Peroxidase for 15 minutes at room temperature and then washed in PBS-T four times for five minutes each. 3,3'-Diaminobenzidine (DAB) Chromogen was diluted with DAB Substrate (1:50 dilution) in restricted light conditions and applied to tissue. DAB produces a brown colour when oxidized by hydrogen peroxide in presence of peroxidase. Tissue was incubated in the slide tray with restricted light for 8 min. Slides were washed with PBS-T four times for five minutes each, then dehydrated and mounted as described above.

2.8 PCR Array for Angiogenic Genes

Total RNA from RV samples of male and female rats subjected to PAB (2 weeks) or sham surgery was extracted using Rneasy Mini kit (Qiagen, ON, Canada) as per the manufacturer's instructions. Briefly, RV (25 mg) samples were placed in in RNAse free sample tubes and buffer RLT containing 10% β-Mercaptoethanol (10 µL buffer per mg of tissue) was added to each sample. Samples were homogenized using bead mill (Cat# 10158- 558, VWR, ON, Canada) at 25 hz for 3 minutes. Samples were centrifuged at 8,000 g for 3 min and supernatant was mixed with equal volume of 70% ethanol. 700 µL mixture was transferred to spin column. RW1 (700 µL) was added to the spin column and centrifuged at 8,000 g for 2 min and this step was repeated 2 more times. Next, 700 µL mixture was transferred to spin column. RW1 (700 µL) buffer RPE was added to the spin column and centrifuged at 8,000 g for 2 min and flowthrough was discarded. Rneasy spin column was then placed in a new 1.5 ml collection tube, 30 µl RNAse-free water was added directly to the spin column membrane and centrifuged at 16,000g for 1 min to collect RNA. RNA quantification was performed by spectrophotometer (absorbance at 260nm). RNA samples were immediately used for cDNA preparation.

cDNA was prepared using High-Capacity cDNA Reverse Transcription Kit (Cat# 4368814, ThermoFisher Scientific, ON, Canada) as per manufacturer's instruction. Briefly, all the samples were diluted to 0.2 µg/µL RNA and 10 µL of sample was added to 10 µL reverse transcription master mix. Reverse transcription was carried out using a thermal cycler (Cat# A24811, Applied Biosystems, ThermoFisher Scientific, ON, Canada) with enzyme activation at 25°C for 10 min, reverse transcription at 37°C for 120 min and reverse transcriptase inactivation at 85°C for 5 min. cDNA was stored at -80°C until used for the PrimePCR array for angiogenic genes (Cat# 10047063, Biorad, ON, Canada). Quantitative RT-PCR was performed using SsoAdvanced™ Universal SYBR® Green Supermix (Cat# 1725272, Biorad, ON, Canada) as per the manufacturer's instructions. qPCR amplification was performed on the Biorad CFX 96 instrument (Biorad, ON, Canada). cDNA products were amplified by first activation at 95°C for 2 min and then for 40 cycles of 5 seconds denaturation at 95°C and 30 seconds annealing at 60°C.

2.9 Primary Endothelial Cell Isolation via Magnetic Sorting

Rat RV endothelial cells (RV-EC) from male and female Fischer CDF rats were isolated as reported previously with some modifications (Pinto et al., 2016). Heart samples from rats were collected post-sacrifice and the RV was separated as described earlier in this thesis. The RVs were each placed onto a clean 10-cm petri dish with 500 µL of Collagenase Dispase (CD) (CAT#:11097113001, Roche Diagnostics, ON, Canada) and minced into small approximately 1 mm^3 pieces using surgical scissors and then collected with an additional 1 mL of CD into a 15 mL falcon tube. Enzymatic digestion of the RV was performed by placing the minced RV sample containing tubes in a 37°C water-bath for 15 min and gently mixing every 3 min. After tissue digestion, the cell suspension and undigested tissue mixture was passed through a 40 µm cell strainer (CAT# 07-201-430 Fisher Scientific, ON, Canada). Unstrained material was returned to the 15 mL Falcon tube containing fresh 1 mL of CD and the enzymatic tissue digestion procedure was repeated. Cell suspensions from the first and second tissue digestion were combined and centrifuged at 400 g for 5 min at 4°C. Extreme care was taken throughout this process to avoid cross-contamination of samples when more than one animal was used. Following centrifugation, the supernatant was aspirated, and the cell pellet was re-suspended in ice cold magnetic sorting buffer and incubated with CD31 antibody (CAT# MAB13937, Millipore, MA, USA; 1:20 dilution) for 30 min. Magnetic sorting buffer was PBS with 3% BSA and 0.58% EDTA by weight.

After the incubation, 1 mL of magnetic sorting buffer was added and the sample was centrifuged at 400 g for 5 min at 4°C. The supernatant was decanted and cells were re-suspended in another 100 µL of ice-cold magnetic sorting buffer. This process was repeated three times total. After the final wash, cells were resuspended in 100 µL ice-cold magnetic buffer and magnetic beads coated with anti-rabbit secondary antibody were added (Miltenyi Biotec, BC, Canada; 1:5 dilution). The sample was incubated for 30 min on ice. Following the incubation, washing was performed three times as described above. The sample was then re-suspended in 1 mL of degassed ice-cold magnetic sorting buffer.

For $CD31^+$ cell sorting, the magnetic sorting columns were primed by passing 500 µL of degassed ice-cold magnetic sorting buffer. Next, the cell suspension was added to the column. Cells were washed 3-times with 1 mL degassed ice-cold magnetic sorting buffer. Then, the columns were removed from the magnet and placed over a fresh collection tube. Fresh degassed ice-cold magnetic sorting buffer (500 µL) was added and a plunger was used to force cells out. Cells were immediately centrifuged at 400 g for 5 min at 4°C and resuspended in 1 mL of Endothelial Growth Media2-MicroVascuature containing 5% charcoal stripped fetal bovine serum (CS FBS) (EGM2-MV; LONZA, ON, Canada). This media and CS FBS concentration was used in all experiments unless otherwise stated. To support the adhesion of freshly isolated RVECs, 300 µL of fibronectin was incubated at 37°C in needed wells of a 24-well plate for at least 30 min and up to 1.5 hours. Fibronectin was removed and the resuspended cells were plated in the fibronectin-coated wells.

RVECs were cultured in a CO_2 incubator at 37°C using EGM-2MV and were monitored for morphology and growth. Endothelial cell colonies were visible within 1-3 weeks. When large colonies became visible, they were passaged and plated into one well of a 6-well plate, followed by a T75 flask.

In all experiments, the passaging procedure was as follows. Cell media was removed and cells were washed with pre-warmed cell culture grade PBS. Cells were incubated at 37°C with pre-warmed trypLE (Cat# 50591420, Gibco, ThermoFisher Scientific, ON, Canada) for 5 min. Following the incubation, cells were physically disturbed by tapping their plate and cell detachment was confirmed by visually inspecting the plate under a microscope. All fluid was transferred to a 15 mL tube and mixed with 1 mL of pre-warmed media. This process was repeated up to three times as needed until all cells were collected. After the final round of trypLE, the plate or flask was washed with PBS and the product was collected again. Cells were then centrifuged at 400 g for 5 min at 4°C, with a soft deceleration to avoid disturbing the cell pellet. The supernatant was removed and cells were re-suspended in 1 mL of pre-warmed EGM2-MV.

2.10 Flow Cytometry

Post-passage, cells were counted using a hemocytometer and approximately 100,000 cells were aliquoted and stained with IgG Isotype Control (eFluor660) or CD31 Invitrogen (eFluor660). For each of two samples, 0.3 µL of IgG Isotype Control or CD31 Invitrogen was added to 100 µL of flow buffer containing the cell suspension. They were incubated on ice and in the dark for 30 minutes. Post-incubation, cells were washed three times using flow buffer. Using the BD FACSDiva and BD FACSCelesa (BD Biosciences, MA, USA) in the Dalhousie University Flow Cytometry CORE, cell surface markers or scatters were analyzed, respectively. Forward scatter and side scatter voltages were set at 630V and 390V, respectively. Voltages for eFluor660 and AF488, were respectively 500V and 440V. Results were analyzed using FlowJo. Gating for $CD31^+$ cells was performed using IgG Isotype controls and blank samples.

2.11 Estradiol Treatment and Angiogenic Gene Expression

Male Fischer CDF RVECs (passage 11-14) were grown in six 6 cm cell culture dishes. Each experiment included 6 treatment conditions. Two plates served as a vehicle control, two were treated with 10 pM Estradiol, and two were treated with 100 pM Estradiol in EGM2 + 2% CS FBS One of each condition was collected at 24 and 48 hr timepoints. Estradiol stock (2 mM) solution was prepared by dissolving 17β-estradiol (Millipore-Sigma, ON, Canada) in anhydrous ethanol. Treatment concentrations were created by diluting the estradiol and ethanol mix with EGM2 + 2% CS FBS. The maximum concentration of ethanol in a treatment was <0.0001% and an equivalent ethanol amount was added in controls. For treatment, the original untreated media was removed, cells were washed with pre-warmed PBS, and then media containing appropriate treatment was added.

mRNA isolation was performed at 24 and 48 hr time-points using Rneasy Mini kit (Qiagen, ON, Canada) as per the manufacturer's protocol. Briefly, 200 µL buffer RLT containing 10% β-Mercaptoethanol was added directly to each plate, cells were scraped with cell scrapers, and the lysate was collected in RNAse free sample tubes. An additional 150 µL of Buffer RLT mixture was added to each plate and they were scraped again. The lysate

was collected, vortexed for 1 min, and the tubes were visually inspected to ensure there was no visible cell matter. Next, 350 µL of 70% ice cold ethanol was added to the homogenized lysate and mixed by pipetting. The sample was transferred to an Rneasy spin column placed in a 2 mL collection tube and centrifuged for 20 sec at 8000 g at 4°C. The flow-through was discarded. From the kit, RW1 was added to each Rneasy spin column and centrifuged for 20 sec at 8000 g and 4°C. The flow-through was discarded. For Dnase digestion, 30 µL Dnase 1 stock solution was added to 210 µL Buffer RDD and mixed by gently inverting the tube and centrifuging for 10 sec at 8000 g. Next, 80 µL of the Dnase 1 incubation mix was added directly to every Rneasy column membrane and incubated at room temperature for 15 min. After the DNAse treatment, buffer RW1 (350 µL) was added to each Rneasy spin column and tubes were centrifuged for 20 sec at 8000 g at 4°C, and the flow-through was discarded. Then, buffer RPE (500 µL) was added to the Rneasy spin column and columns were centrifuged at 8000 g for 20 sec and the flow-through was discarded. This step was repeated twice. The Rneasy spin column was transferred to a new 2 mL collection tube and centrifuged for 1 min at 8000 g and 4°C. The Rneasy spin column was transferred to a new 1.5 mL collection tube and 20 µL of RNAse-free water was added to the spin column membrane and incubated on benchtop for 4 min. The sample was centrifuged for 1 min at 8000 g and 4°C.

Samples were placed on ice and mRNA quality and quantity were immediately assessed using an Ultraviolet Spectrometer. Samples were loaded in duplicates onto a BioTekTake3 Micro-Volume Plate (CAT# 22605, BioTek, USA). Samples with 1.5 µg or more of mRNA with a 260 over 280 ratio between 1.90 and 2.10 were converted into cDNA using High Capacity cDNA Reverse Transcription Kit (ThermoFisher Scientific, ON, Canada) as per manufacturer's protocol. For each reaction, 10 µL of master mix was added to a combined 10 µL mix of mRNA and Rnase-free H_20 for a total concentration of 2 µg mRNA/20 µL. cDNA was stored at -80°C until used for RT-qPCR.

Using the PrimePCR ASSAYS and PANELS guide from BioRad, 1 µL of 20x PrimePCR Assay, 10 µL of 2x SsoAdvanced Universal Supermix, 8 µL of nuclease free water, and 1

µL of cDNA were mixed in a sample tube for each gene investigated. From BioRad, PrimePCR SYBR Green Assay, Desalt 200R primers for the genes SPHK1, CTGF, and TGFβ2 (CAT #: 10025636) were used and two replicates were completed for every sample. HPRT1 was used as the reference gene (Table 1).

Table 2: Primer information for genes of interest investigated using RT-qPCR

Primer name	Unique Assay ID
Sphk1	qRnoCED0003979
Tgfβ2	qRnoCID0006448
Fgf6	qRnoCED0005605
Ctgf	qRnoCED0001593
Hprt1	qRnoCED0057020

Samples were centrifuged and run through the thermal cycler to facilitate cDNA synthesis. Following the PrimePCR Assay Quick Guide (BioRad), the PCR cycling protocol consisted of a 2 min 95°C activation stage, followed by 39 repeat cycles of a 5 sec 95°C denaturation stage and 30 sec 60°C annealing/extension stage. Upon completion of the final annealing/extension stage, a melt curve commenced where samples were exposed to 65°C and the temperature increased incrementally by 0.5°C every 5 sec until the temperature reached 95°C.

To calculate ΔΔCq, first, Cq mean was determined for each gene of interest using two technical replicates and ΔCq was calculated by subtracting the reference gene (HPRT1) mean Cq from the mean Cq of our gene of interest. Next, for each gene of interest, mean control ΔCq was calculated by averaging the ΔCq from all control samples for that gene. ΔΔCq was calculated by subtracting the mean control ΔCq from individual controls and treated sample mean ΔCqs. Finally, $2^{(-\Delta\Delta Cq)}$ was calculated for each trial and the averages were plotted.

2.12 Network Formation Assay

Matrigel assays, a type of network formation assay, were performed using male Fischer CDF RVEC (passage 12-14). In preparation for an experiment, Matrigel (Corning, CA,

USA) was placed in the 4°C fridge overnight to thaw. Angiogenic slides (CAT# 81506, Ibidi, Germany.) and pipette tips were placed in the freezer overnight to cool and prevent gelling of the Matrigel during plating.

At the beginning of the experiment, cell media was removed and RVECs were washed with PBS, and then starved using Endothelial Basal Media 2 (EBM2) +0.5% CS FBS for 4 hr. During this time, the thawed Matrigel was kept on ice and plated (10 µL) in each of the lower wells of the angiogenic slide. The Matrigel was incubated at 37°C for at least 30 min and at most 1.5 hr before cells were plated on top.

Following the starvation, RVECs were harvested and plated in each well of angiogenic slides (15,000 cells in 25 µL), and an additional 25 µL of media (EBM2+0.5% CS FBS) containing treatments (vehicle, 10 pM or 100 pM estradiol) were added. Following treatment, cells were incubated at 37°C in CO_2 incubator and imaged at 0, 12, 24, and 48 hrs using a LMI-3000Series Routine Inverted Microscope (LAXCO, Belgium) with the SeBaCam Digital Camera (PN:SeBACam100, Laxco, WA, USA) at 10x magnification. Images were analyzed using WimTube, a network formation quantification tool provided by Wimasis Image Analysis. The completed analyses included detailed information regarding Branching Points, Total Loops, Tube Length, and Covered Area.

2.13 Statistical Analyses

Analyses with 3 or more groups were done using ordinary one-way ANOVA and Sidak's multiple comparisons test, with a single pooled variance. Analyses with 2 groups were tested for normality using the Shapiro-Wilk test analysis and then a t-Test assuming a Gaussian Distribution, unless otherwise specified. Analyses were performed by GraphPad Prism (version 9.3.1) and statistical significance was set at $p<0.05$. All error bars show standard deviation. All figures were formatted in BioRender.

CHAPTER 3: RESULTS

3.1 Female Fischer CDF Rats Demonstrate Adaptive Right Ventricular Remodelling Compared to Maladaptive Remodelling in Male Rats at 2 Weeks Post-PAB

3.1.1 PAB-Induced RV Pressure Overload was Similar in Male and Female Rats

At baseline, there were no significant differences in RVSP and RV hypertrophy (RVH) between male and female Fischer CDF rats (Figure 4A, 4B). PAB resulted in significant increase in RVSP in male and female rats; however, there was no significant difference in RVSP and RVH between males and females at 1-week and 2-week time-points, suggesting that PAB resulted in similar increases in afterload between male and female rats.

It is important to note that age-matched littermate male and female rats were utilized in this study and male rats had significantly higher body weight than female rats (Figure 4C). The differences in body size may impact PA diameter between male and female rats; therefore, we assessed PA diameter of sham male and female rats using echocardiography. As expected, males had larger mean PA diameters compared to female rats (3.1 mm ± 0.2 mm and 2.7 mm ± 0.3 mm, respectively) (Figure 4D). However, the difference in PA diameter and animal size between sexes did not appear to significantly influence RV afterload as RVSP and RVH were similar at 1-and 2-week time-points between male and female rats (Figure 4A and 4B). Moreover, the differences in PA diameter did not translate into significant differences in PA percent occlusion (Figure 4E). Using PA diameter, we calculated the circle area of the PA and gauge used to determine what percent of the PA was restricted by PAB (Equation 1). At 1-week post-PAB, male and female rat PA percent occlusion was 76.8% and 78.2%, respectively. At 2-weeks post-PAB, male and female rat PA percent occlusion was 77.8% and 77.3% (Figure 4E). Overall, data suggests that the PAB procedure was successful in inducing RV pressure overload.

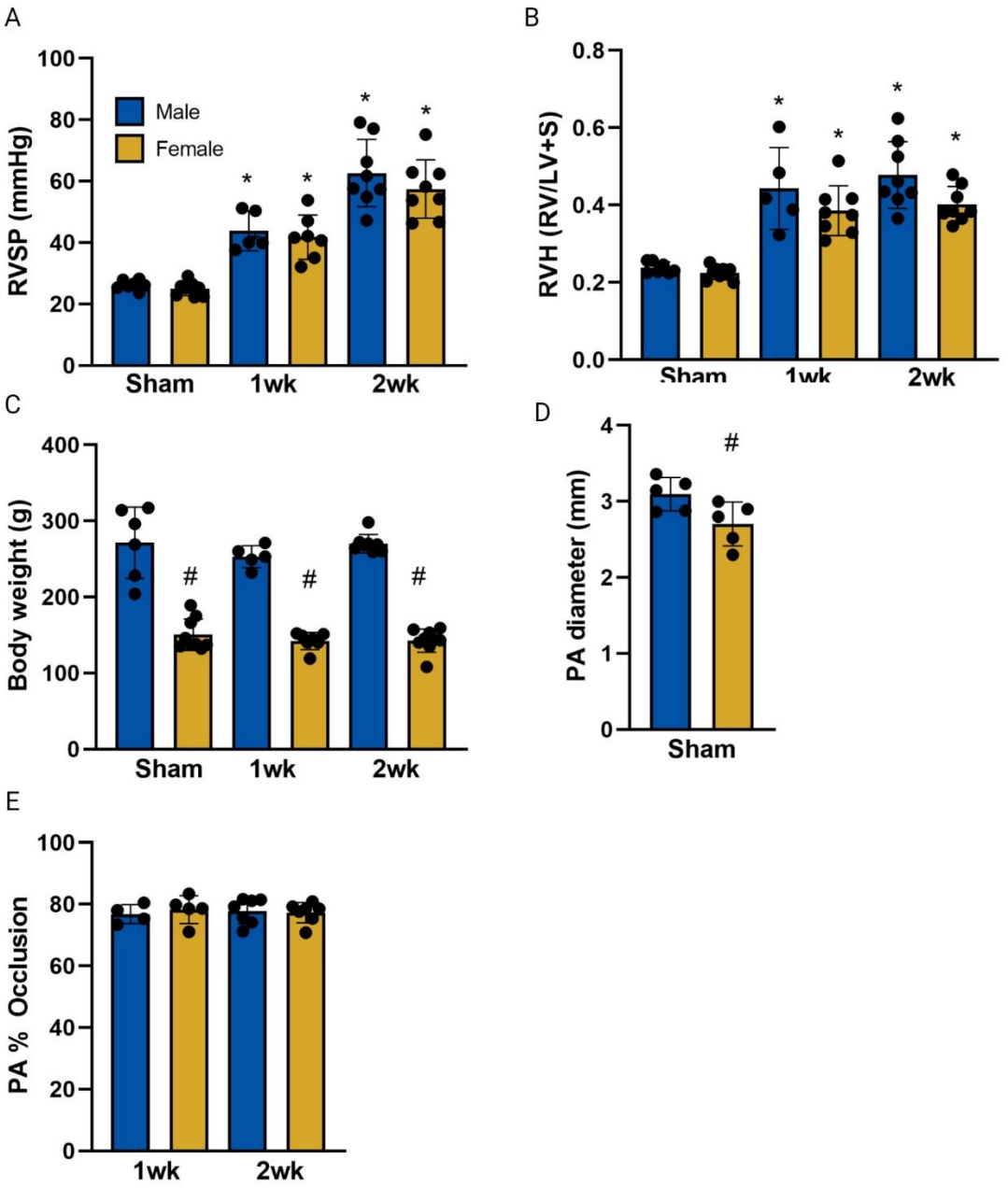

Figure 4: PAB successfully increased afterload in male and female rats. Right ventricular systolic pressure (mmHg) (n=5-9) **(A)** and right ventricular hypertrophy (n=5-9) **(B)** were increased in male and female rats at 1- and 2-weeks post-PAB compared to respective sham groups. At all timepoints males were significantly heavier than females (n=5-9) **(C)**. Pulmonary artery diameter (n=5) **(D)** was higher in male than female sham rats. There were no sex differences in percent occlusion of the right ventricle (n=4-7) **(E).** Ordinary one-way Anova and Sidak's multiple comparisons test with a single pooled variance were used for all analyses of groups of 3 or more. Normality for pulmonary artery diameter was tested using the Shapiro-Wilk test and then a t-test assuming a Gaussian Distribution**.** #p<0.05 vs male at the same time point. *p<0.05 vs naïve of the same group. Error bars are standard deviation.

3.1.2 Echocardiography Assessment of Early Changes in Right Ventricle Function and Structure Showed Sex Differences in Rats Subjected to PAB

Female rats exhibited better cardiac function than males at 1- and 2-weeks post-PAB as demonstrated by higher SV index and CI (Figure 5A, 5B). No significant difference was observed in SV index and CI between naïve male and female rats (Figure 5A and 5B). HR was unchanged in response to PAB and similar in both sexes at all time-points and in naïve rats (Figure 5C). Additionally, female PAB rats showed greater RV FS than males at 1-week post-PAB (Figure 5D). There was a trend towards declining FAC in male rats at 2-weeks post-PAB that was not seen in females (Figure 5E). Females had a stronger tricuspid annular plane systolic excursion than males at the 1-week timepoint (Figure 5F).

There were significant structural sex differences in response to PAB. Males had a significant increase in RV dilation, observed as an increase in RVIDd/LVIDd and RVIDd and that was not observed in females (Figure 6A and 6B) and a trend towards an increase in RVIDs (Figure 6C). RVAWd was increased in males 1-week post-PAB and increased in males and females 2-weeks post-PAB (Figure 6D). This data matches our RVH data and further reinforces that hypertrophy was similar between male and female rats. There were no significant changes in RVAWs (Figure 6E).

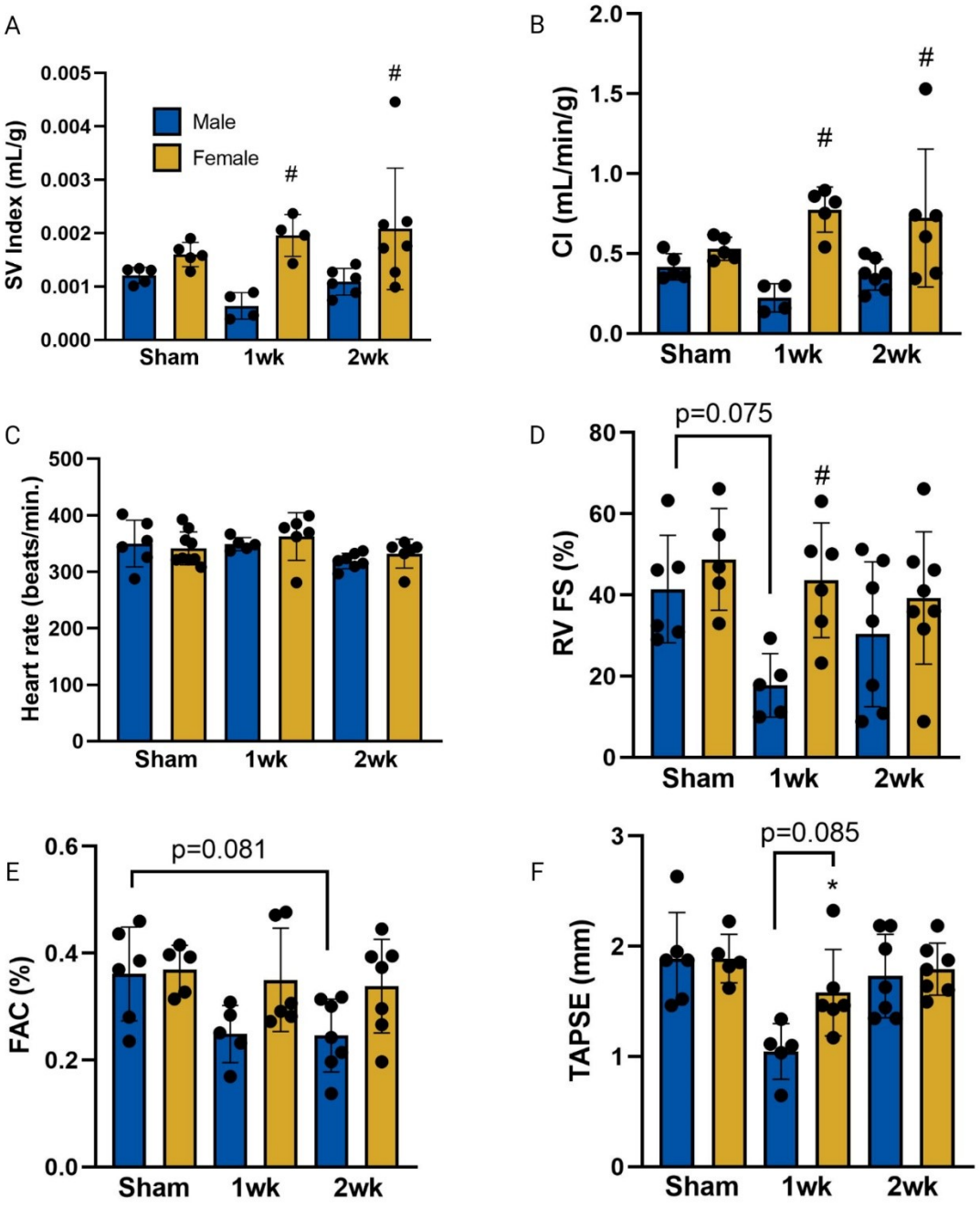

Figure 5: Females maintained stronger heart function than males in response to PAB. Stroke volume index (n=4-7) **(A)** and cardiac index (n=4-7) **(B)** were significantly higher in females than males at the 1- and 2-week timepoints. There were no observed changes in heart rate (n=5-9) **(C)**. RV fractional shortening (n=5-8) **(D)** and fractional area change (n=5-7) **(E)** were trending towards a decline in male PAB animals compared to sham. Tricuspid annular plane systolic excursion was equal between groups (n=5-7) **(F)** Statistical tests used were ordinary one-way ANOVA and Sidak's multiple comparisons test, with a single pooled variance. *p<0.05 vs naïve of the same group. Error bars are standard deviation.

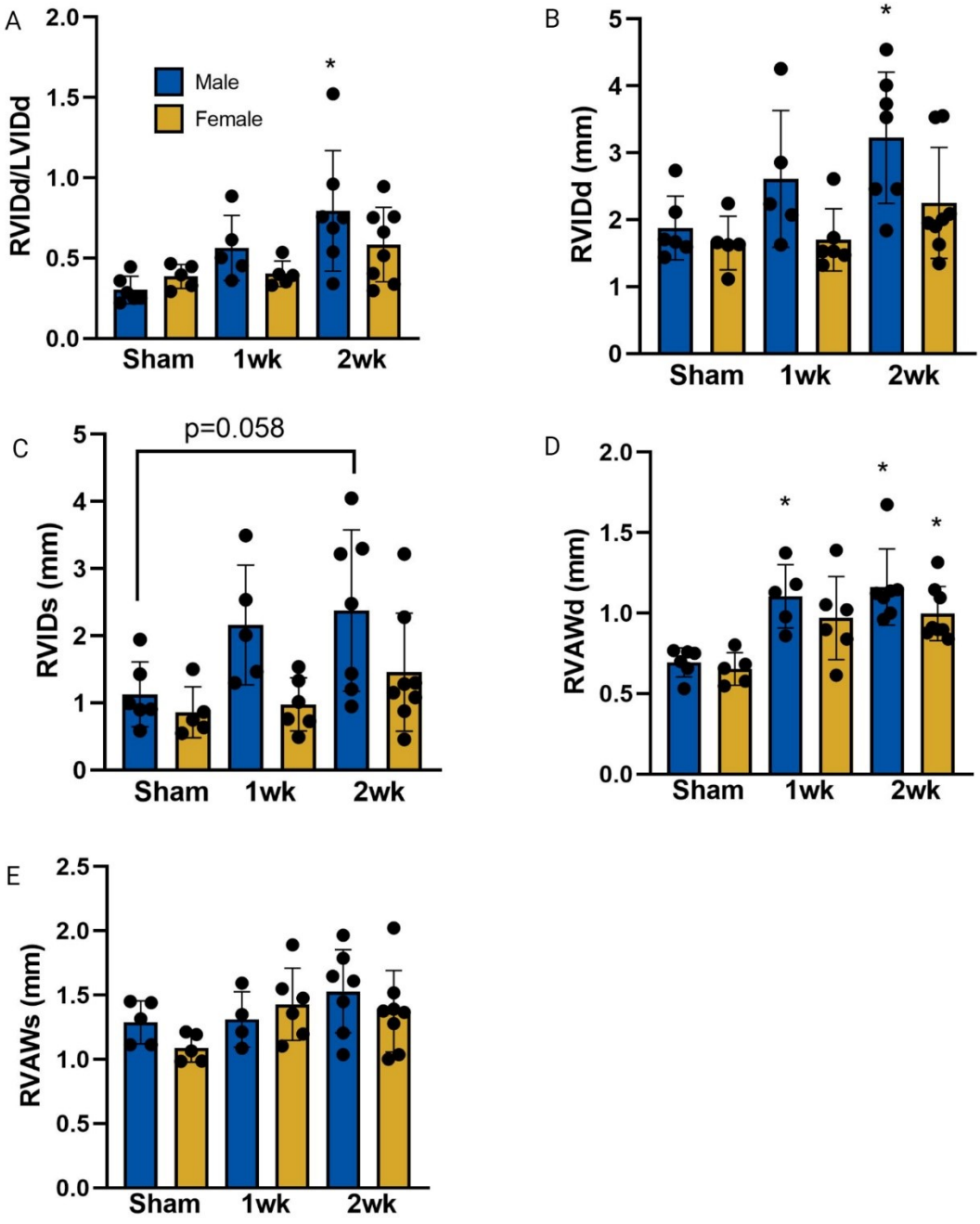

Figure 6: Male rats 2-weeks post-PAB exhibited structural markers of maladaptation in response to PAB while female structure was largely maintained. RVIDd/LVIDd (n=5-8) and RVIDd (n=5-8) **(A, B)** were increased in males 2-weeks post-PAB**.** There was a trend towards a decline in male RVIDs post-PAB (n=5-9) **(C)**. RVAWd was increased in males 1-week post-PAB and increase in males and females 2-weeks post-PAB (n=5-8) **(D)** There were no changes in RVAWs (n=4-8) **(E)**. Statistical tests used were ordinary one-way ANOVA and Sidak's multiple comparisons test, with a single pooled variance *p< 0.05 vs naïve of the same group. Error bars are standard deviation.

3.1.3 Histological Assessment of Right Ventricle Remodelling of Male and Female Fischer CDF Rats Subjected to PAB

In response to PAB, male Fischer CDF rats demonstrated an increase in cardiomyocyte CSA at 1- and 2-weeks post-PAB. Cardiomyocyte CSA did not change significantly in Fischer female rats subjected to PAB and males had a significantly higher cardiomyocyte CSA than females at 2-weeks post-PAB (Figure 7).

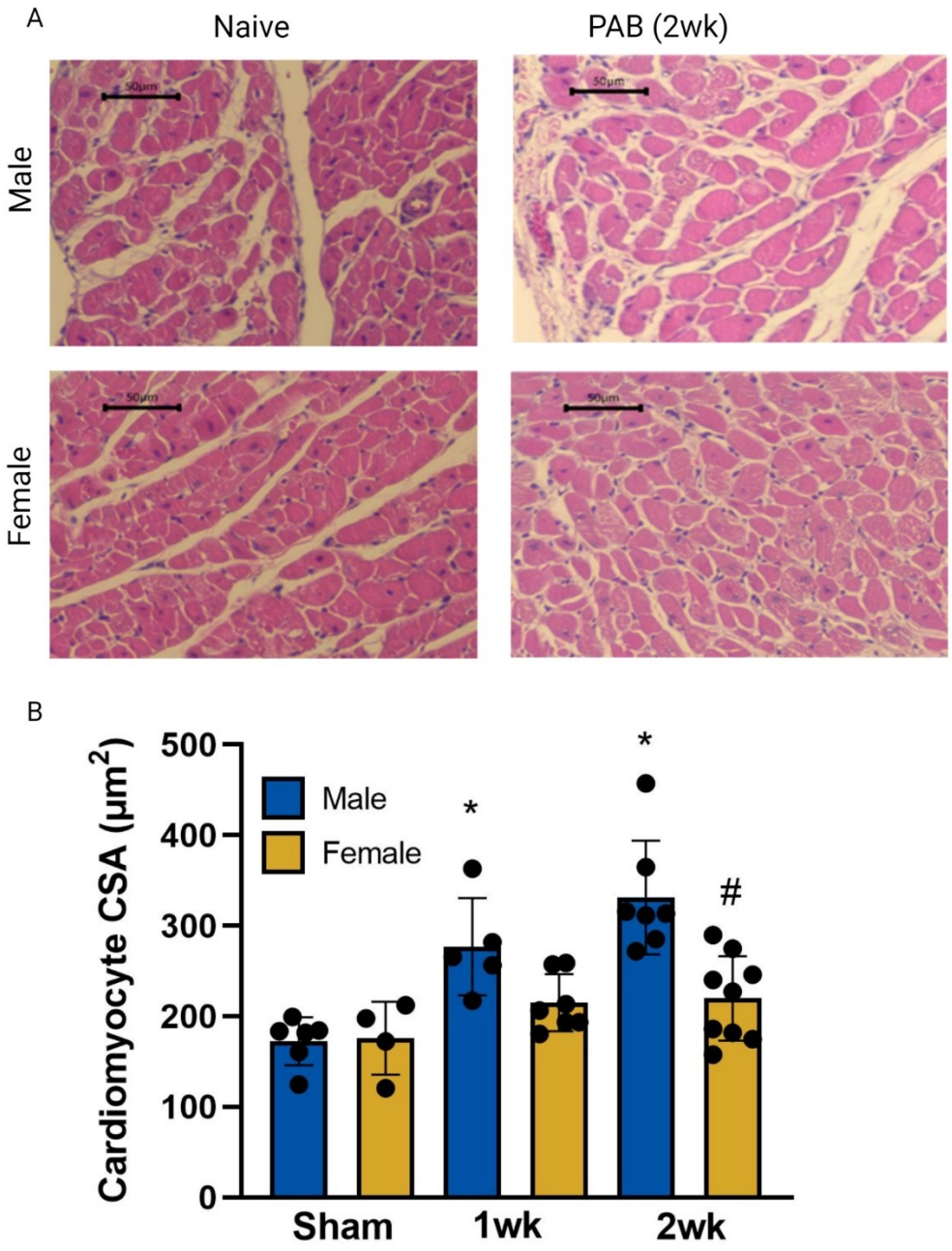

Figure 7: Representative images of hematoxylin and eosin staining of RV sections from male and female, naive or 2-week post-PAB rats **(A)**. Graph showing mean cross sectional area of RV cardiomyocytes in male and female, naive and PAB rats (n=4-9) **(B)**. Statistical tests used were ordinary one-way ANOVA and Sidak's multiple comparisons test, with a single pooled variance *p< 0.05 vs naïve of the same group. #p<0.05 vs male of the same time point Error bars are standard deviation.

3.1.4 Up-Regulation of Angiogenic Gene Expression in the Right Ventricle of Female Rats Compared to Male Rats Following PAB

Previous studies have reported that RV angiogenesis plays a role in RV remodelling (Potus et al., 2015). Adequate RV angiogenesis during RV remodelling in response to increased RV afterload has been demonstrated to be associated with adaptive RV remodelling with maintained RV function and structure, while inadequate RV angiogenesis has been linked to maladaptive RV remodelling (Suen et al., 2019).

Therefore, we performed a PCR array focused on 86 angiogenic genes using RV samples of male and female Fischer CDF rats subjected to PAB or sham surgery. Tissue from PAB groups was used from the 2-week time-point. At 2 weeks post-PAB, we observed an up-regulation of angiogenic genes in the female RVs compared to male RVs (Figure 8). Out of 84 angiogenic genes studied in PCR array, 35 genes were significantly up regulated in female rat RVs compared to male rat RVs (Table 3). Overall, these results suggested that differential angiogenesis could play a role in sex differences in RV adaptation in response to PAB.

Following up on results of the angiogenic gene PCR array, we assessed von Willebrand Factor (vWF) expressing cells as a surrogate for vascular density in the RV. No significant difference in EC density was observed in the RV of male and female Fischer CDF rats subjected to sham surgery or 1- and 2-week timepoints post-PAB (Figure 9).

Table 3: Angiogenic gene expression in the female rat RVs relative to male rat RVs at 2 weeks post-PAB. Log 2-fold change PAB female compared to male PAB animals at the 2 weeks timepoint. Females had a significantly higher upregulation of 86 known angiogenic genes

Gene	Log 2 (Fold change PAB female to PAB male)	-Log p
MMP14	1.7906	2.6515
Itgb3	0.7156	2.5510
Itga5	0.5188	2.5137
Serpinf1	1.7586	2.3486
Vegfb	-0.5633	2.2824
Igf1	1.1598	2.2110
Angpt2	1.0420	2.1808
Tgfb2	**2.2678**	**2.1480**
Epas1	-0.6450	2.1214
Anpep	1.1153	2.0580
MMP2	1.1962	2.0280
Nrp2	1.3532	2.0260
Ctgf	**2.4924**	**1.9311**
Edn1	1.7703	1.9283
MMP3	1.2765	1.9139
Fgf1	-0.6785	1.8560
Tgfa	0.9989	1.8206
MMP19	0.8092	1.8106
Mdk	0.8032	1.7992
Fn1	0.9123	1.7388
Figf	1.4927	1.7343
Angpt1	-1.8156	1.6888
Col18a1	1.0858	1.6317
Fgf6	**2.7238**	**1.5783**
Gusb	0.6118	1.5491
Vegfa	-0.2384	1.3672
Ptgs1	0.3962	1.3639
Hgf	0.8134	1.3376
Timp2	0.6651	1.3264
Sphk1	**2.0186**	**1.3026**
Pgf	0.7828	1.2218
Itgav	0.5075	1.2019
Tgfb1	0.4530	1.1183
Vegfc	0.4550	1.1172
Timp1	1.0698	1.0852

Gene	Log 2 (Fold change PAB female to PAB male)	-Log p
Fgfr3	-0.6008	1.0782
Cxcl2	0.8230	0.9443
Tgfb3	0.9069	0.9239
Thbs1	0.8993	0.9131
Lect1	2.2781	0.8560
S1pr1	0.4529	0.7992
Hif1a	0.3581	0.7560
Efna1	-0.3493	0.7364
Mapk14	0.3569	0.7053
Hsp9/Oab1	-0.2321	0.6833
Tek	-0.2759	0.6816
Lep	0.9057	0.5969
Serpin1	-0.5872	0.5431
Ifng	-0.6859	0.5284
Serpinb5	1.0975	0.5091
Tie1	0.2818	0.4938
Cdh5	0.2316	0.4600
Ptk2	0.1686	0.4497
Egf	1.5713	0.4365
Il1b	0.3099	0.4310
Pdgfb	0.1943	0.4271
MMP9	1.4348	0.3863
Pecam1	0.1349	0.3792
Cxcl9	0.2589	0.3743
Plau	0.1836	0.3693
Tgfbr	0.2229	0.3628
Ifna1	0.7551	0.3614
Tnf	-0.4335	0.3560
Akt1	-0.0918	0.2820
Tymp	0.8987	0.2811
Ccl2	-0.3266	0.2808
Ifnb1	0.6680	0.2757
Eng	0.1216	0.2483
Ang	0.1775	0.2373
Cxcl1	-0.1969	0.2179
Pdgfa	0.1597	0.2174
Il6	0.2567	0.2106

Gene	Log 2 (Fold change PAB female to PAB male)	-Log p
Bal1	0.1874	0.1786
B2m	-0.0589	0.1737
Timp3	0.1117	0.1726
Erbb2	0.1208	0.1607
Jag1	0.1180	0.1473
Nrp1	0.0824	0.1353
Col4a3	0.0715	0.0771
Id1	-0.0534	0.0689
Plg	0.0361	0.0491
Kdr	0.0307	0.0438
Fgf2	0.0397	0.0378
Nos3	0.0150	0.0349
Tbp	0.0201	0.0330
F3	-0.0070	0.0072

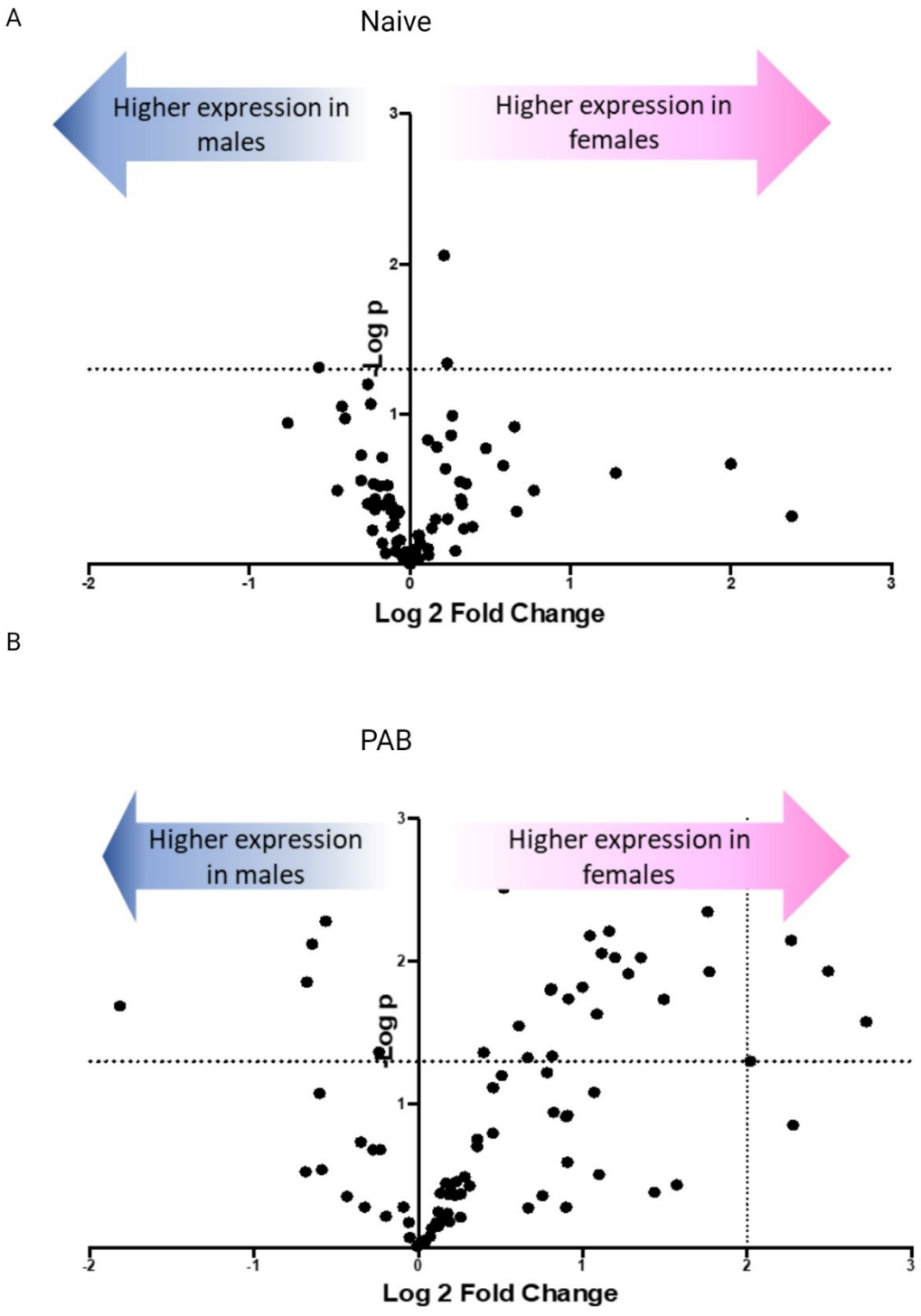

Figure 8: Volcano plots demonstrating relative expression of 84 known angiogenic genes in the RV of female rats compared to male rats 2-weeks following sham **(A)** or PAB surgery **(B)**.

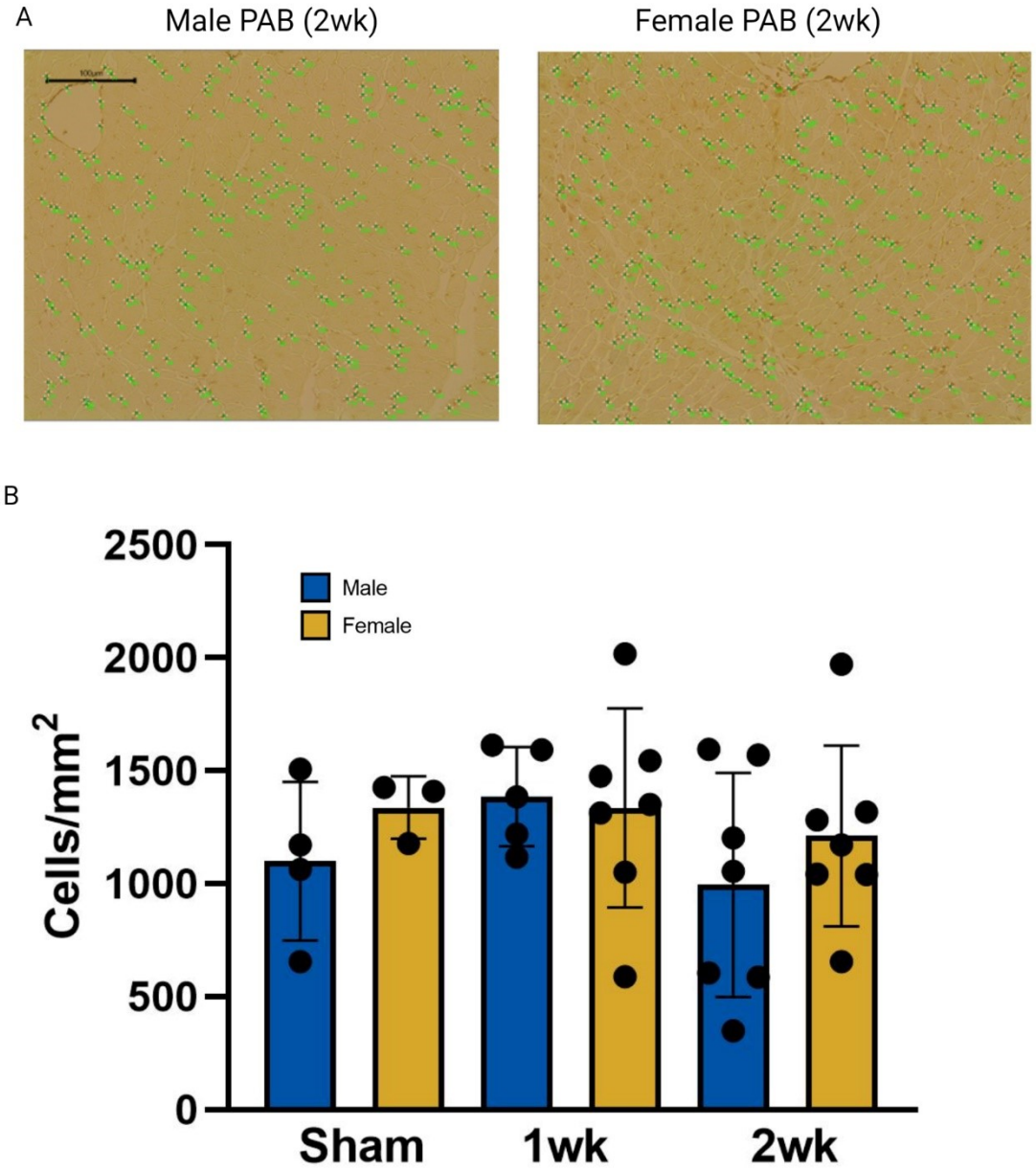

Figure 9: There were no sex differences or change in vWF expression between PAB and sham groups **(A)** Representative images of vWF cell counts 2-weeks post-PAB using ImageJ Multi-point tool. Scale bar is 100 µm and consistent between both images. **(B)** vWF positive cell counts in sham rats and PAB 1-, and 2-weeks post-surgery (n=3-7). There were no differences between groups. Statistical tests used were ordinary one-way ANOVA and Sidak's multiple comparisons test, with a single pooled variance. Error bars are standard deviation.

3.1.5 Echocardiography Assessment of Late Changes in Right Ventricle Structure and Function Showed No Sex Differences in Rats Subjected to PAB

To assess the sex differences in response to prolonged exposure to pressure overload, we extended the studies to 4 weeks post- PAB. Similar to the 2-week study, we did not observe significant sex differences in RVSP and RVH at 4 weeks post-PAB (Figure 10A, 10B). The only measure with a significant sex difference at the 4-week timepoint was body weight (Figure 10C). There were no significant differences in PA occlusion between male and female rats (Figure 10D). There were no changes in other structural markers of RV adaption including RVIDd/LVIDd, RVIDd, and RVIDs (Figure 10E, 10F, 10G). Regarding functional markers of RV adaptation, there were no significant sex differences in FAC, SV Index, CI, HR, TAPSE, and RV FS at the 4-week timepoint (Figure 11A, 11B, 11C, 11D, 11E and 11F). Lastly, Cardiomyocyte CSA, was not statistically different. Between male and female groups (Figure 11G).

3.1.6 Echocardiography Assessment of Ovariectomized Female Rats Showed no Differences in Rats Treated with Estradiol

To assess the role of estradiol in the adaptations observed in female rats, we performed PAB on OVX females and treated one group with estradiol. In the OVX condition, there were no significant differences in RVH and RVSP between treated and untreated groups (Figure 12A, 12B). Treated rats had lower body weight than untreated rats (Figure 12C). Structurally, there were no significant differences in RVIDd/LVIDd, RVIDd, and RVIDs (Figure 12D, 12E, 12F). Regarding functional markers of RV adaptation, there were no significant sex differences in FAC (Figure 13A). SV Index was significantly higher in treated rats (Figure 13B). There were no significant differences in CI and HR between treated an untreated group (Figure 13C and 13D). There was also a trend towards reduced TAPSE in the estradiol treated group (Figure 13E). Lastly, there were no significant differences in RV FS and Cardiomyocyte CSA between groups (Figure 13F and 13G).

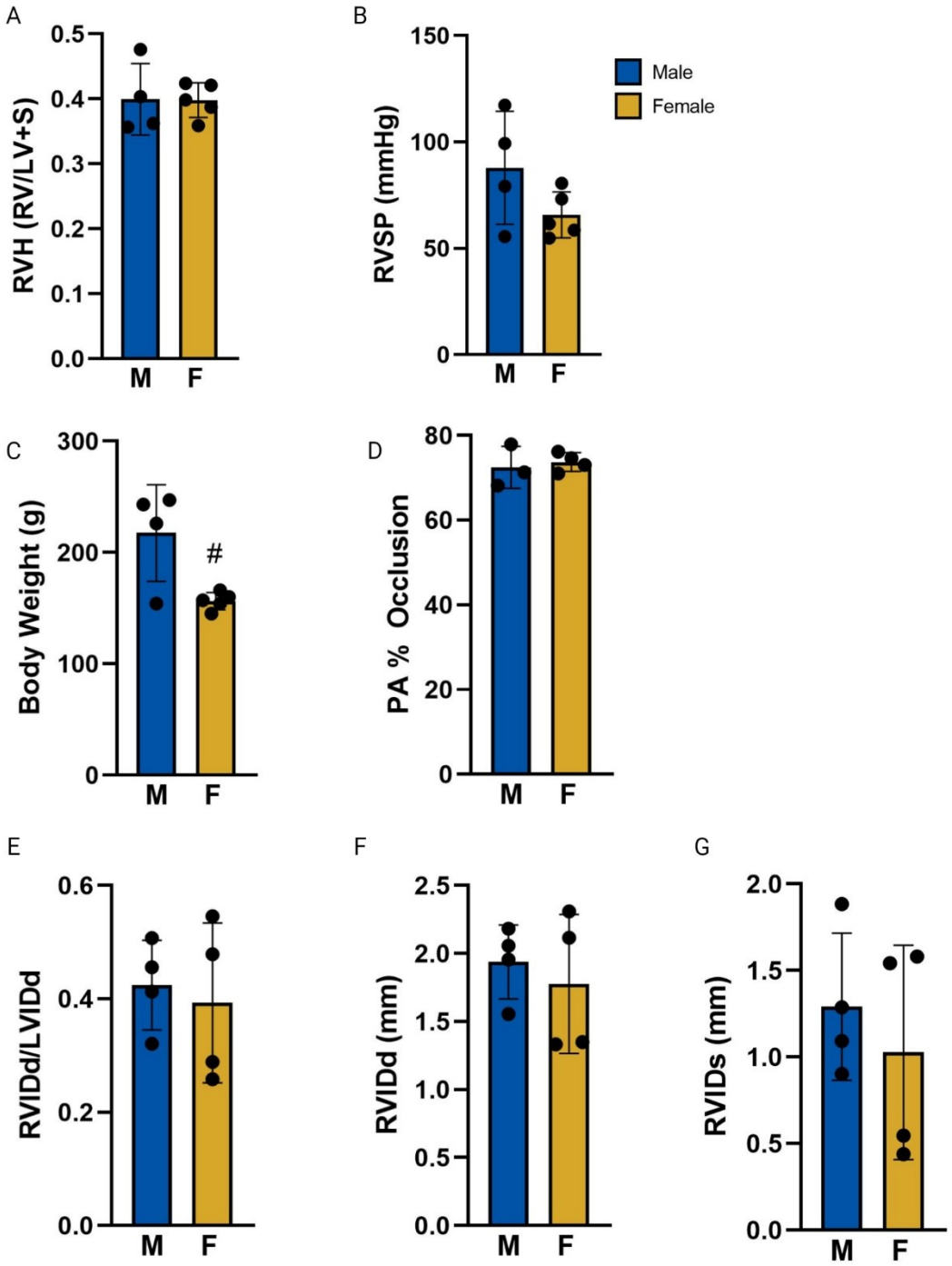

Figure 10: There were no significant sex differences in RVH (n=4-5) **(A)** and RVSP (n=4-5) **(B)** 4-weeks post-PAB**.** Body weight was significantly higher in males (n=4-5) **(C)**. There were no sex differences in PA % Occlusion (n=3-4) **(D)**, RVIDd/LVIDd (n=4) **(E)**, RVIDd (n=4) **(F)**, and RVIDs (n=4) **(G)** between male and female rats. Normality was tested using the Shapiro-Wilk test and then a t-test assuming a Gaussian Distribution was performed. #p<0.05 vs male of the same time point. Error bars are standard deviation.

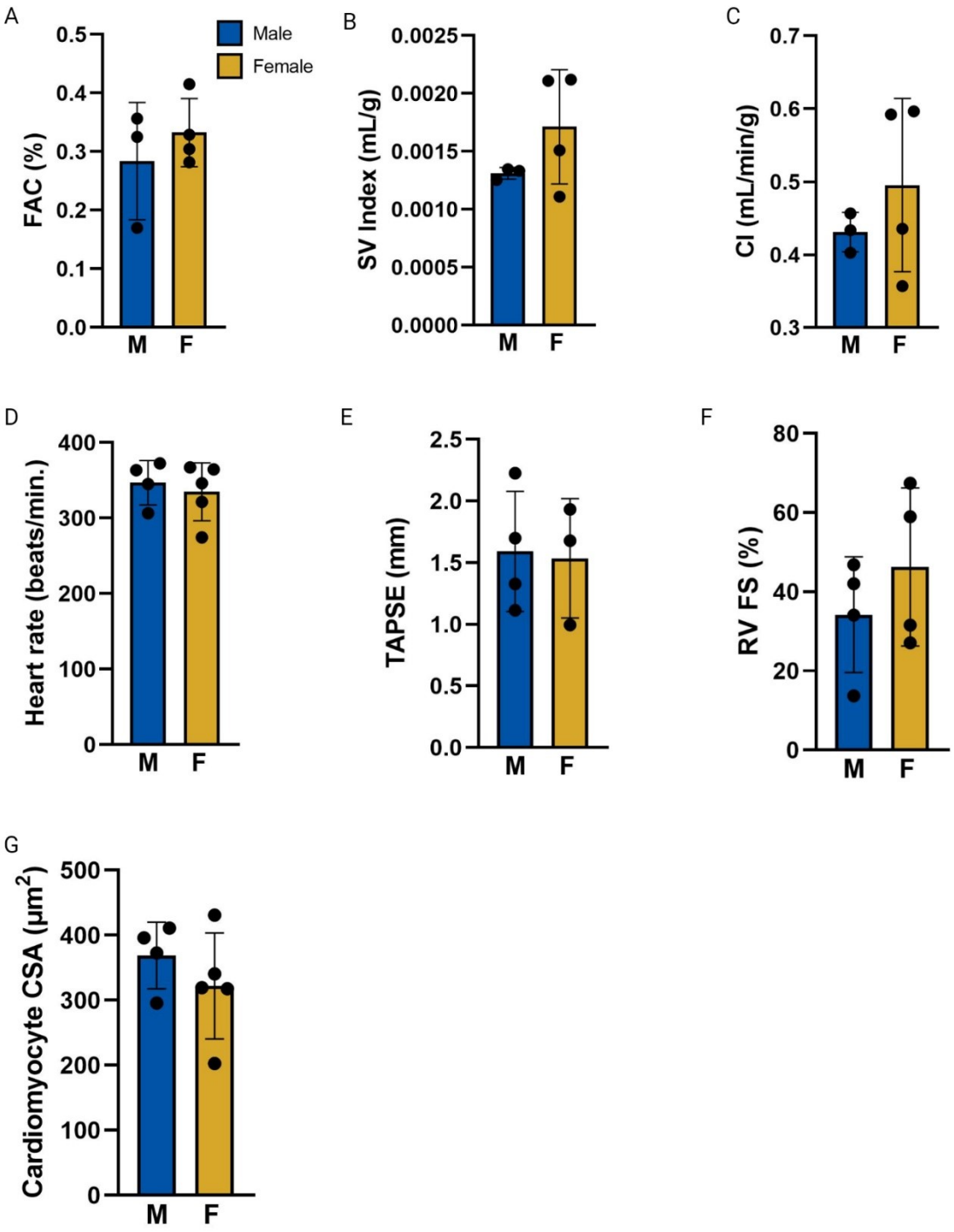

Figure 11: There were no significant sex differences in FAC (n=3-4) **(A)**, SV Index (n=3-4) **(B)**, cardiac index (n=3-4) **(C)**, heart rate (n-4-5) **(D)**, TAPSE (n=3-4) **(E)**, FS (n=4) **(F)** and cardiomyocyte CSA (n=4-5) **(G)** 4-weeks post-PAB. Normality was tested using the Shapiro-Wilk test and then a t-test assuming a Gaussian Distribution was performed. #p<0.05 vs untreated. Error bars are standard deviation.

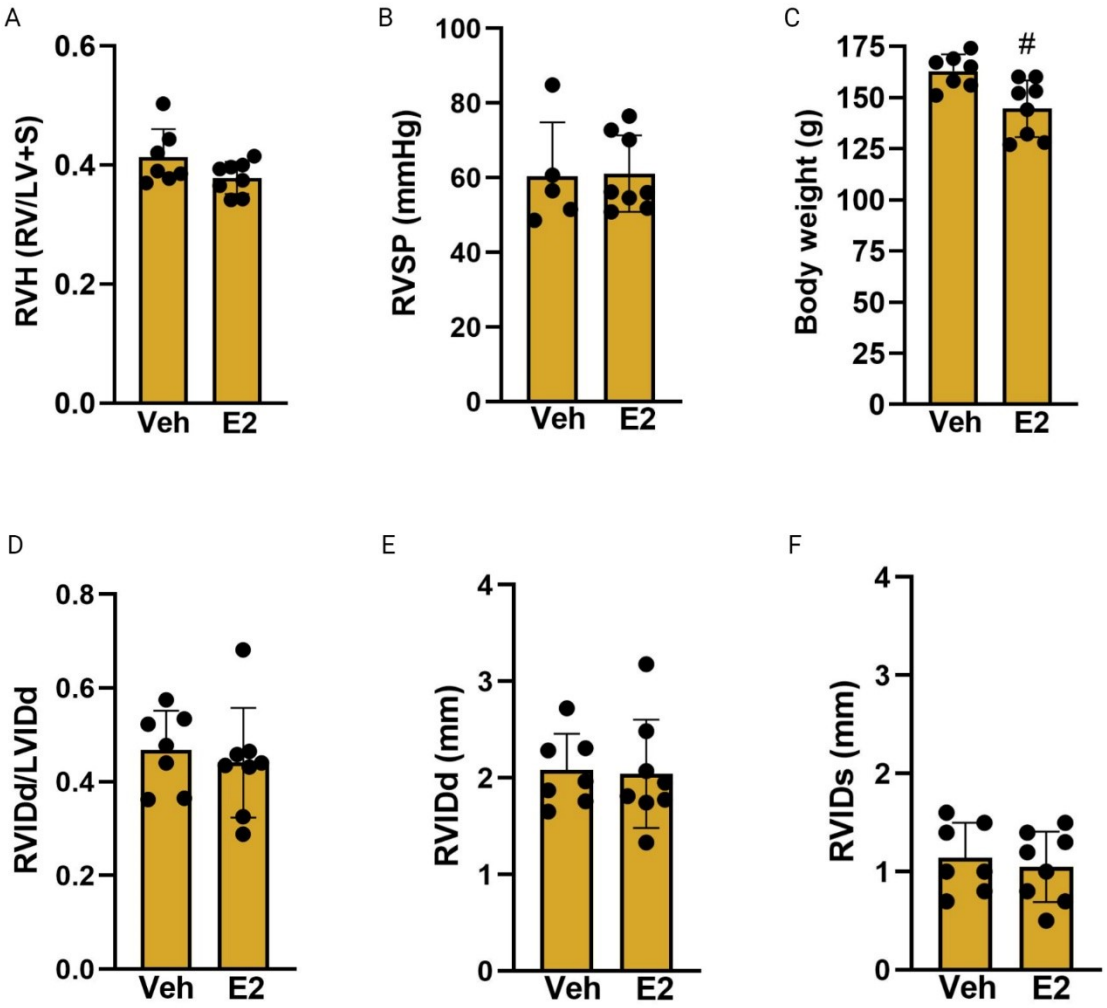

Figure 12: In OVX females at 2-weeks post-PAB, there were no significant differences between treated and vehicle groups' RVH (n=7-8) **(A)** and RVSP (n=5-8) **(B).** Body weight which was significantly higher in the vehicle group compared to the treated group **(C).** RVIDd/LVIDd (n=7-8) **(D)**, RVIDd (n=7-8) **(E)**, and RVIDs (n=7-8) **(F)** were not statistically different between groups. Normality was tested using the Shapiro-Wilk test and then a t-test assuming a Gaussian Distribution was performed. #p<0.05 vs male of the same time point. #p<0.05 vs untreated. Error bars are standard deviation.

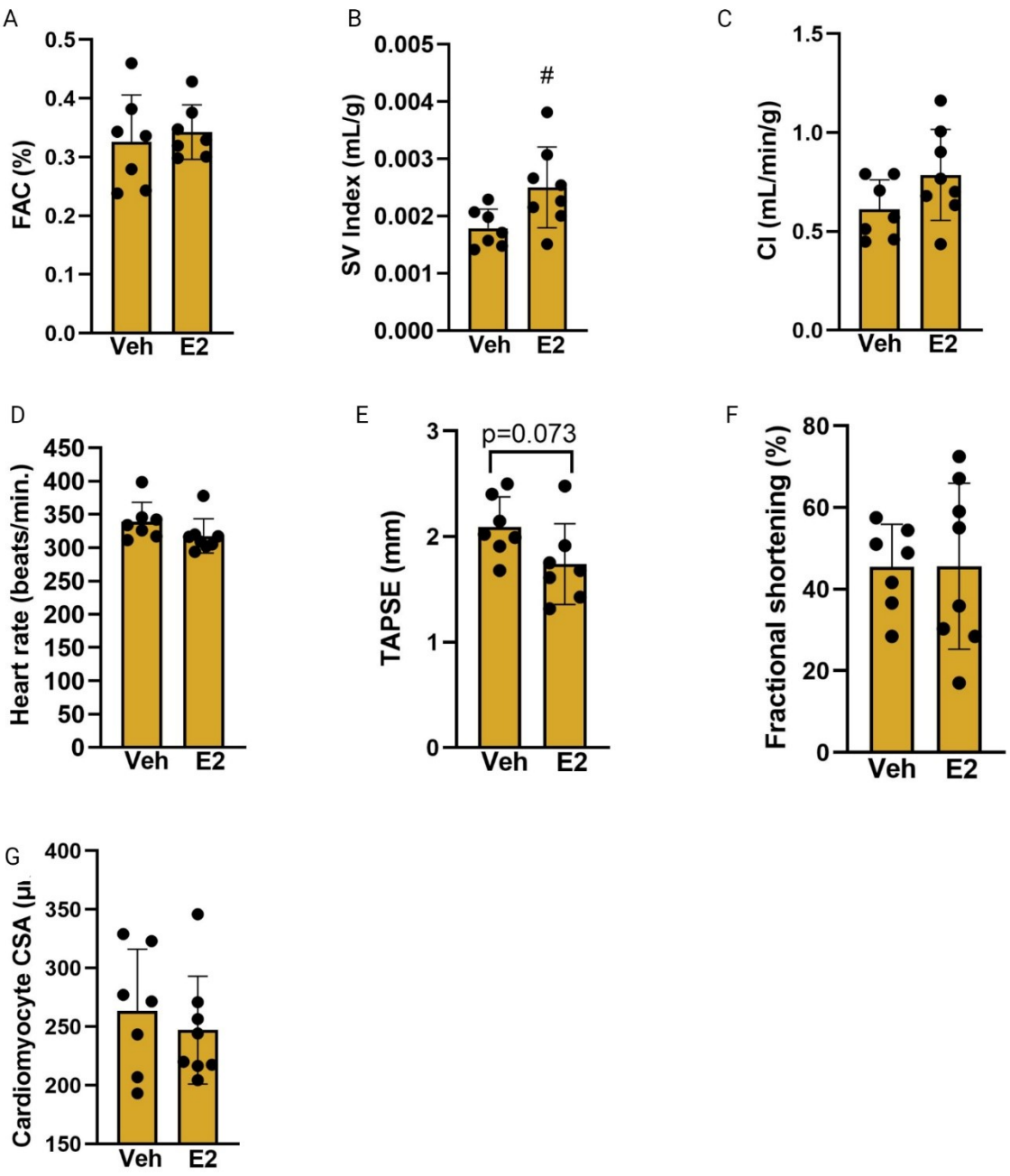

Figure 13: In OVX females at 2-weeks post-PAB, there were no significant differences in FAC (n=3-4) **(A).** The estradiol treated condition had a significantly higher SV Index than the vehicle group (n=7-8) **(B)**. There were no significant differences in cardiac index (n=7-8) **(C)** and heart rate (n=7-8) **(D)**. There was a trend towards a decrease in TAPSE in the estradiol group (n=7) **(E).** There were no statistical differences in fractional shortening (n=7-8) **(F)** and cardiomyocyte CSA (n=7-8) **(G).** Normality was tested using the Shapiro-Wilk test and then a t-test assuming a Gaussian Distribution was performed for all analyses except heart rate because data failed the normality test. #p<0.05 vs untreated. Error bars are standard deviation.

3.2 Effect of Sex on Angiogenic Ability of Fischer CDF Rats

To understand sex differences in early RV remodeling and RV angiogenesis, we assessed the expression of known angiogenic genes in male and female PAB and naïve RV tissue. We also isolated RVECs to further examine possible mechanisms ex vivo. RVECs were isolated from male Fischer CDF rats. Flow cytometry analysis confirmed that 99.6% of female cells (Figure 14A) and 99.3% of male cells (Figure 14B) expressed the endothelial specific cell marker CD31.

3.2.1 Female Sex was Associated with the Upregulation of Known Pro-Angiogenic Genes in Right Ventricular Tissue

The expression of known 86 angiogenic genes (Table 3) was examined using RT-qPCR and tissue collected from female RV and male RV at 2 weeks post-PAB (Figure 8). Interestingly, Sphingosine Kinase 1 (SPHK1), Transforming growth factor-β-2 (TGFβ2), and Connective Tissue Growth Factor (CTGF) expression was more than 2-fold higher in females than males, suggesting a stronger angiogenic response in females compared to males in response to PAB.

3.2.2 Estradiol Did Not Upregulate Known Angiogenic Genes in Male Right Ventricular Endothelial Cells

To examine the potential role of estradiol in the observed upregulation of SPHK1, TGFβ2, and CTGF, expression of these genes was assessed in primary male RVECs following 24 and 48 hr treatment with vehicle, 10 pM or 100 pM E2. Cell morphology was examined visually at each time point, the cells demonstrated typical endothelial cobblestone morphology and estradiol treatment did not alter cell morphology of RV-EC (Figure 15). RT-qPCR data demonstrated that there were no significant changes in SPHK1 and CTGF gene expression in male Fischer CDF cells treated with estradiol for 24 or 48 hours compared to vehicle controls (Figure 16). There was a down regulation in TGFβ1 treated with estradiol at the 24-hour timepoint (Figure 16).

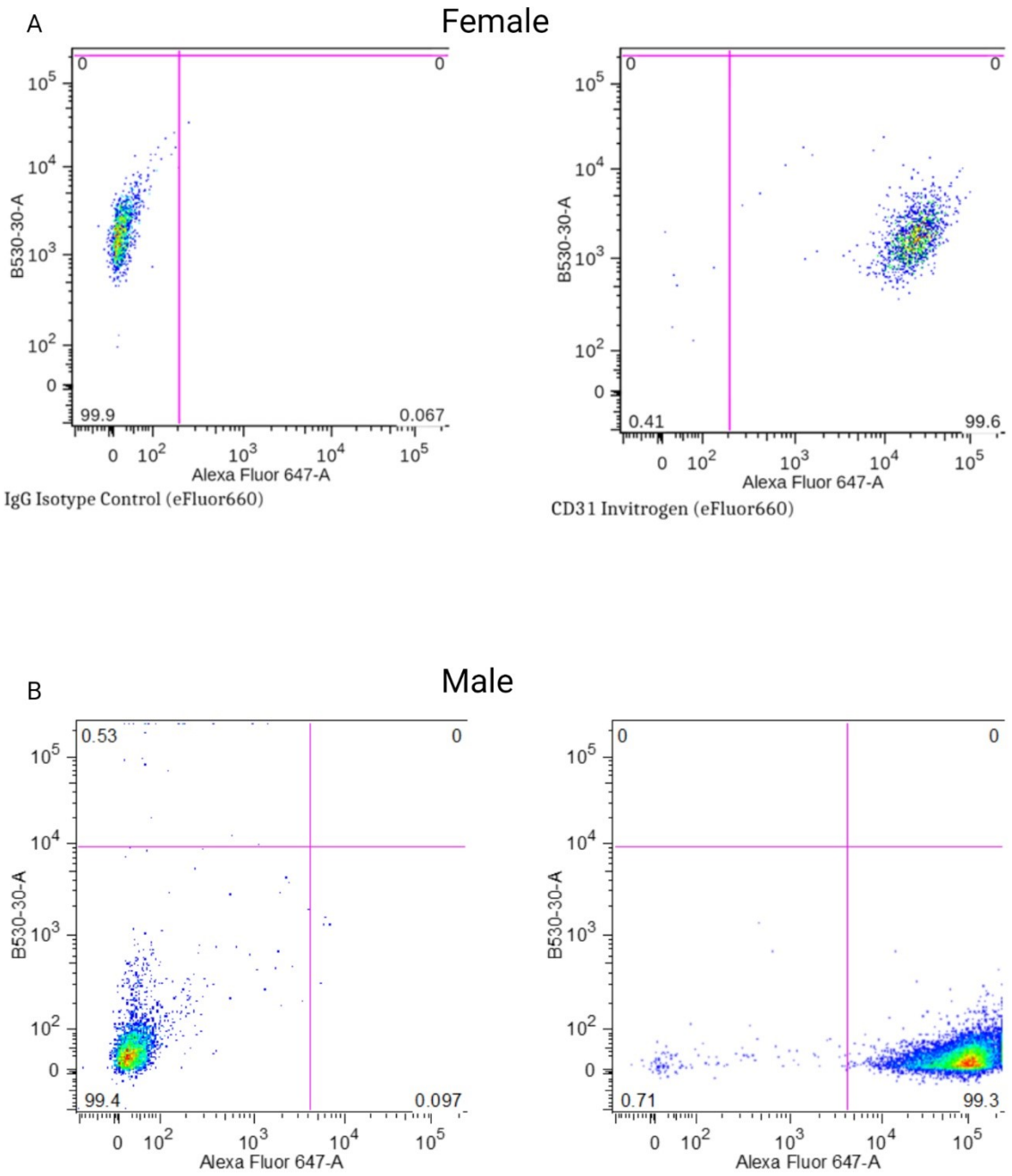

Figure 14: Flow cytometry confirmed that cell samples were endothelial cells. Flow cytometry results for female primary endothelial RVECs. Staining done with IgG Isotype control and gate included 99.9% of sample **(A)**. CD31 Invitrogen was used to stain endothelial cells and 99.6% of cells stained positive **(B).**

A

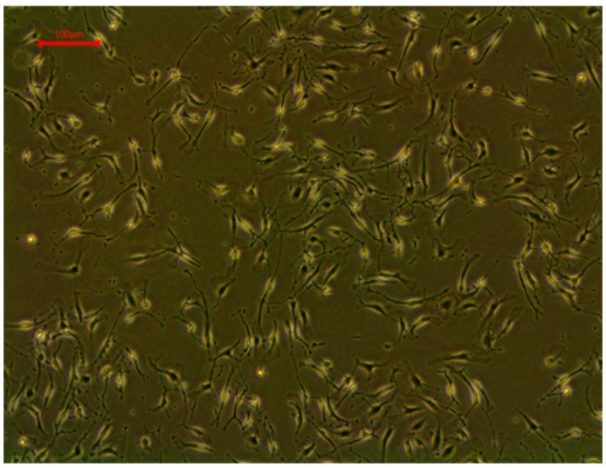

B

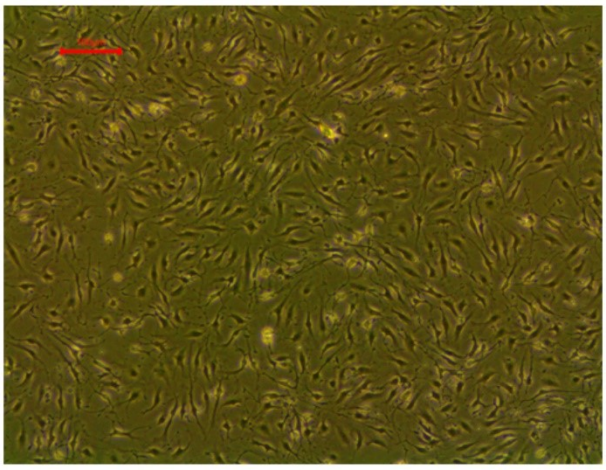

C

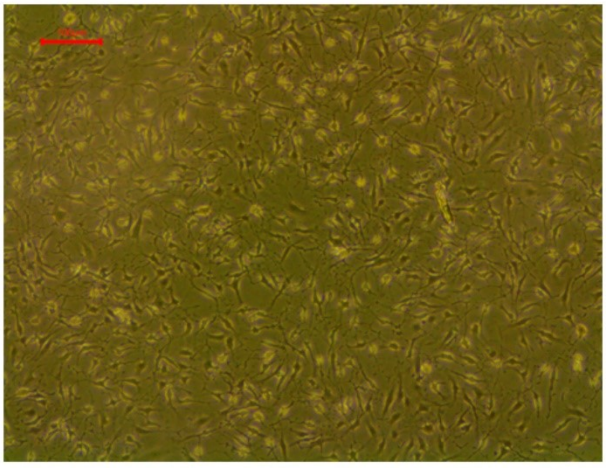

Figure 15: Representative images of male Fischer CDF RVECs at 0hr **(A)**, 24hr **(B)**, and 48hrs **(C)** post-treatment with E2 or vehicle control. Images were taken immediately before mRNA isolations.

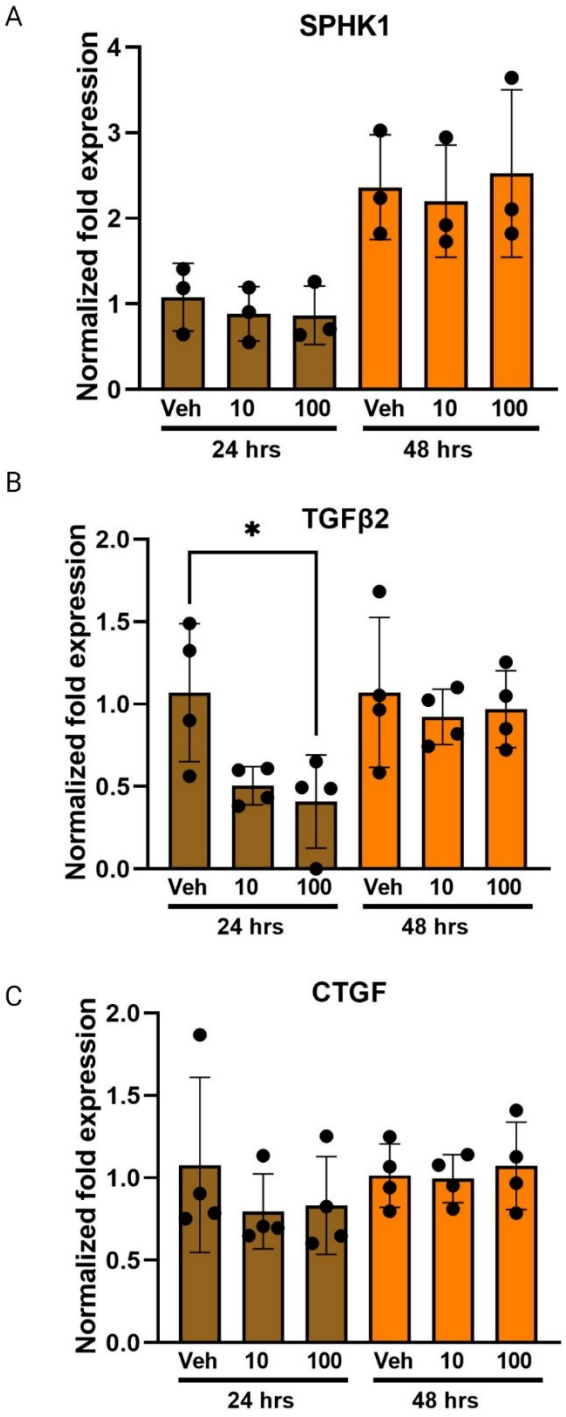

Figure 16: Normalized gene expression for **(A)** SPHK1 (n=2), **(B)** TGFβ2 (n=3), and **(C)** CTGF (n=3) in primary male Fischer CDF RVECs that have been cultured in media containing 10pM and 100pM estradiol concentrations for 24- or 48-hours. Statistical tests used were ordinary one-way ANOVA and Sidak's multiple comparisons test, with a single pooled variance. No statistical tests were performed on SPHK1 because it was under powered. *$p<0.05$ compared to Vehicle. Error bars are standard deviation.

3.2.3 Estradiol Was Associated with an Early Increase in Network Complexity

We observed that cells treated with 100 pM and 1 nM E2 had significantly more Branching Points (Figure 17, 18 and 19A) and Total Loops (Figure 17, 18 and 19D) compared to the Vehicle control at the 12-hour timepoint. There were no significant differences in Total Length or Covered area between groups at the 12-, 24-, or 48-hour timepoints (Figure 20). This suggests that E2 was associated with the early development of complex network formation.

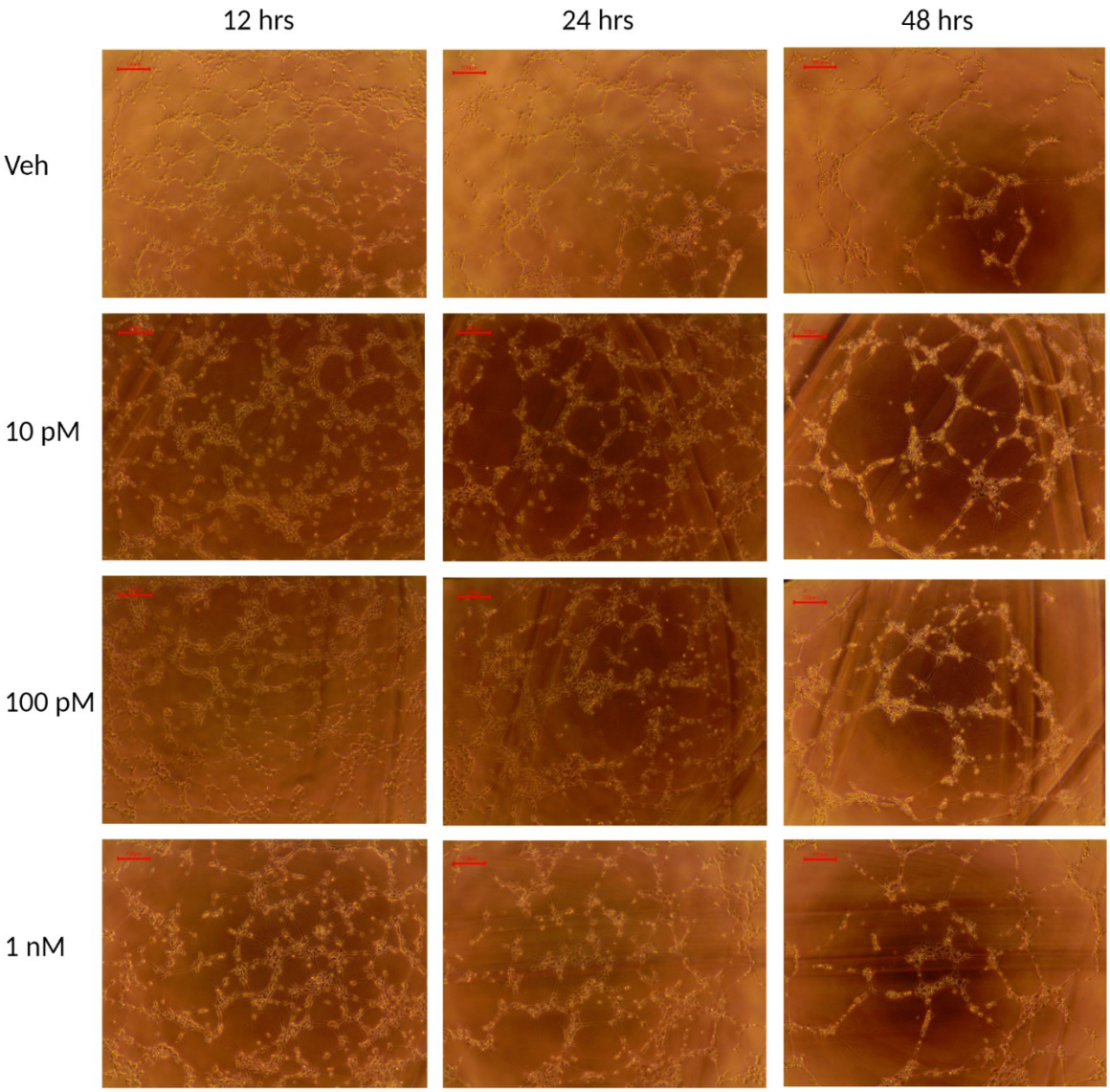

Figure 17: Representative images of Matrigel assays taken at 12, 24, and 48 hours post-plating using male Fischer CDF RVECs. Scale bar is 100 µm.

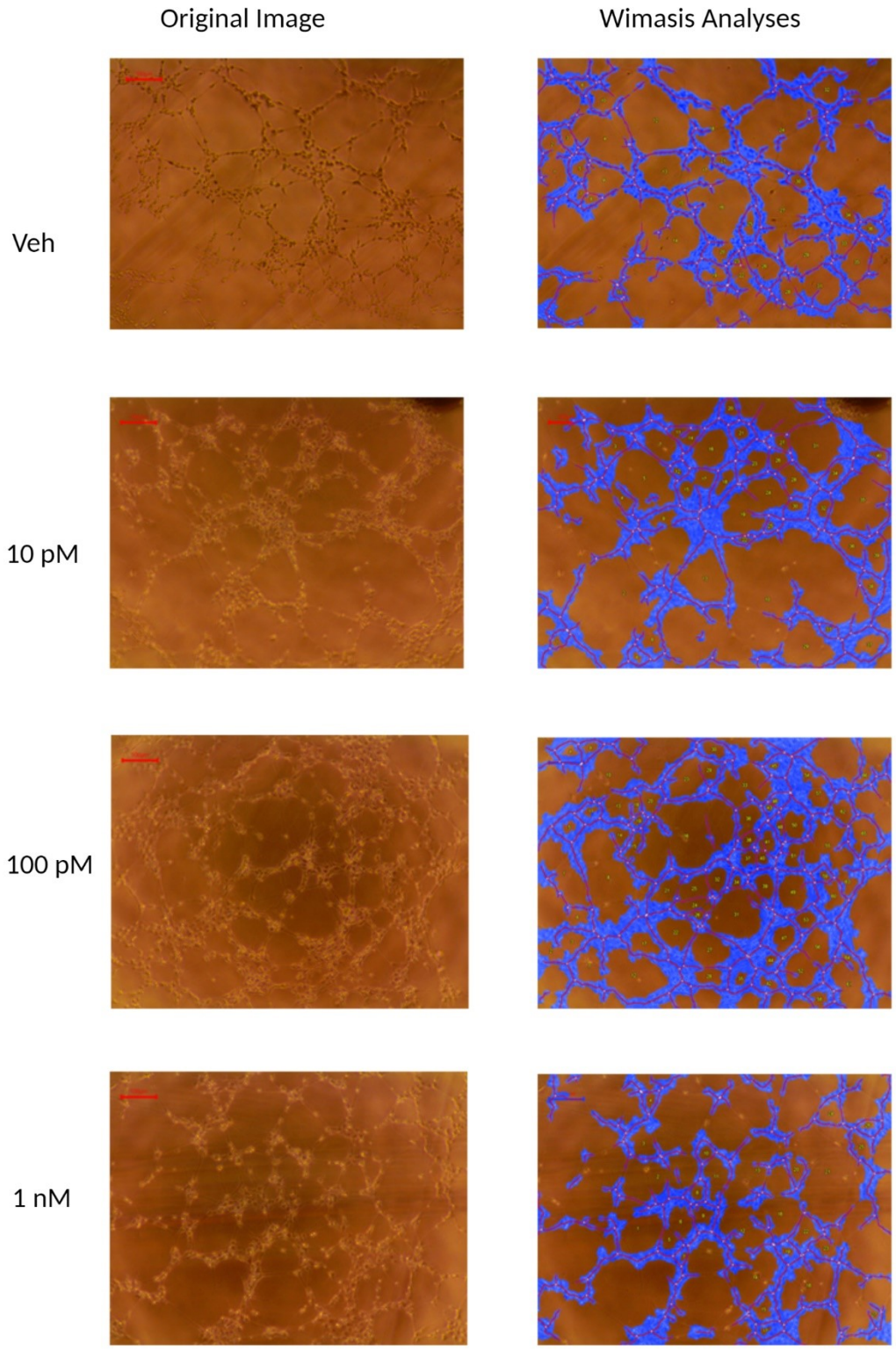

Figure 18: Representative images of Matrigel assays using RVECs taken at 24 hours and completed analyses using Wimasis software. Blue represents area covered in cells or branches. Red lines represent networks/tubes.

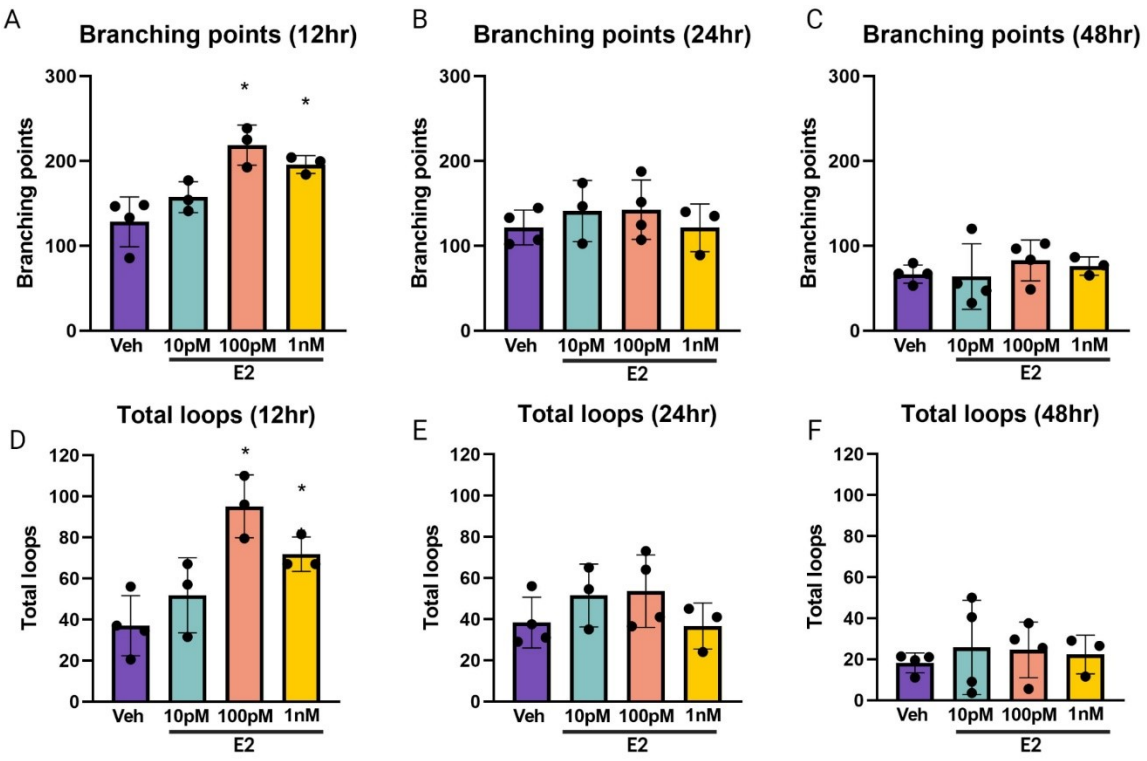

Figure 19: Estradiol treatment (100 pM) treatment was correlated with a significant increase in network complexity at the 12 hr timepoint. There was a significant increase in branching points 12 hrs post-treatment with 100 pM and 1 nM estradiol compared to the vehicle group **(A)**. There were no differences in branching points observed 24 hrs and 48 hrs post-treatment **(B, C)**. There was a significant increase in total loops 12 hrs post-treatment with 100 pM and 1 nM estradiol compared to the vehicle group **(D)**. There were no differences in total loops observed 24 hrs and 48 hrs post-treatment **(E, F)**. Statistical tests used were ordinary one-way ANOVA and Sidak's multiple comparisons test, with a single pooled variance. *$p<0.05$. Error bars are standard deviation.

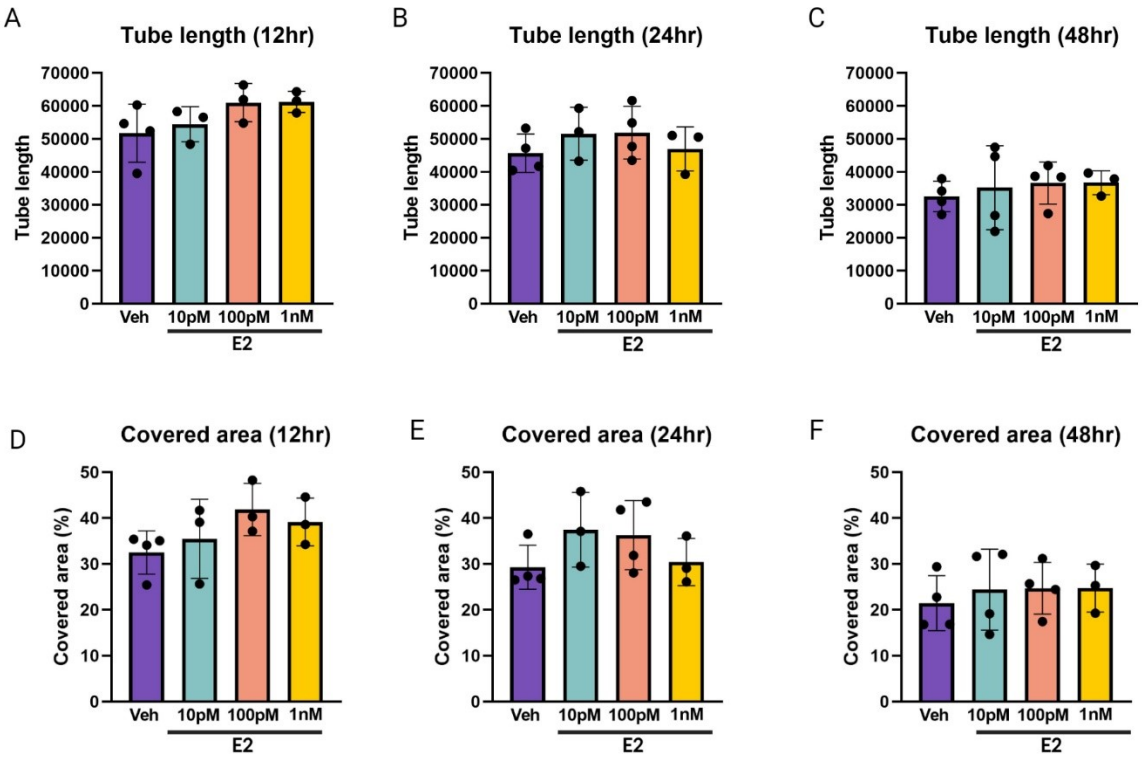

Figure 20: Estradiol treatment (100 pM) treatment was not associated with any changes in tube length **(A, B, C)** or covered area **(D, E, F)** at 12-, 24-, or 48-hours post-estradiol treatment. Statistical tests used were ordinary one-way ANOVA and Sidak's multiple comparisons test, with a single pooled variance. Error bars are standard deviation.

CHAPTER 4: DISCUSSION

4.1 Results Summary and Relevance

This thesis investigated the sexual dimorphism in RV remodeling and development of RHF in Fischer CDF rats PAB model. In response to PAB, male rats demonstrated maladaptive RV remodeling whereas female rats developed adaptive RV remodeling and maintained RV function. We also demonstrated important differences in angiogenic gene expression in the RV of female versus male rats exposed to 2 weeks of PAB. Our data further demonstrated that estradiol treatment increased angiogenic ability of RVEC. Overall, data presented in this thesis demonstrate marked sex differences in RV remodeling in response to increased afterload and identified RV angiogenesis as one of the mechanisms underlying these differences.

Sex differences have been reported in the outcome of the conditions that lead to RHF. For example, clinical data clearly show that females have better prognosis following a PAH diagnosis than males (Foderaro & Ventetuolo, 2016; McGoon & Miller, 2012; van de Veerdonk et al., 2016; Yoo, 2018). Similarly female HfpEF patients have better survival compared to their male counterparts (Duca et al., 2018). It is important to note that better RV function is associated with better survival in PAH and HFpEF patients ((Burke et al., 2014); therefore, better survival in female patients may involve better ability to preserve RV function in response to elevated afterload. Indeed, studies have shown female PAH patients have better RV function and better survival (Swift et al., 2015). Consistent with these observations, at the 2-week timepoint, structurally females had no significant change in RV size, as shown by RVIDd/LVIDd, while males had a significant increase in RVIDd at 2-weeks. Furthermore, at cellular level males also had increased cardiomyocyte CSA compared to the sham group that was not observed in female rats. Functionally, females maintained a higher CI than males post-PAB. Overall, hemodynamic and histological data showed that female Fischer CDF rats functionally and structurally adapted in response to PAB and males exhibited markers of maladaptation. These early changes in Fischer CDF rat PAB model mirror the sexual dimorphism in RV remodeling in human patients and understanding the mechanisms of sex differences in RV adaptation in this model may provide novel insight into the sex differences in pathophysiology of RHF.

Previous research investigating the sex differences have shown protective effect associated with female sex in various animal models including MCT, SuHx and PAB. Frump et al. demonstrated that female SD rats maintained better RV function in repones to SuHx compared to male rats and the protective effects were absent in OVX female rats (Frump et al., 2015). Importantly, estradiol supplementation restored in OVX female rats supplemented with estradiol confirming the protective role of estradiol against RV remodeling in SuHx model (Frump et al., 2015). Similarly, a recent study by the same group reported that estradiol supplementation was protective against SuHx and PAB induced RV remodeling (Frump et al., 2021). In our study, we aimed to investigate the sex differences in RHF susceptible Fischer CDF rats using the PAB model to avoid the influence of female sex on pulmonary vascular disease and investigate the specific effect on the RV. Contrary to previous report, we did not see a major impact of OVX and estradiol replacement on RV remodeling and RV function in our studies. It is important to note that PAH is progressive in SuHX model as compared to the PAB model. Moreover, PAB model in the previous study included estradiol treatment over 7 weeks as opposed to only 2 weeks treatment in the present study. These differences together with RHF susceptibility of Fischer CDF rats may explain the differences in results between earlier studies and our study. Further experiments involving long-term follow-up and estradiol replacement are needed to confirm role of estradiol in RV remodeling in Fischer CDF rats.

Multiple mechanisms have been proposed to be involved in maladaptive RV remodeling and development of RHF including metabolic shift from glucose oxidation to glycolysis, fibrosis, inflammation, and lack of adequate angiogenic response. A landmark paper has demonstrated that RV angiogenesis is a key differentiating event between adaptive and mal-adaptive RV remodeling (Potus et al., 2015). RVECs isolated from patients with decompensated RV remodeling and RHF had reduced angiogenic potential compared to the healthy subjects and patients that demonstrated compensated RV remodeling. The study further demonstrated that mechanisms leading to increased RV angiogenesis could be targeted to improve RV remodeling and prevention of RHF. Furthermore, Frump et al. recently demonstrated the role of estradiol-ERα-apelin signalling in RV angiogenesis and protection against RHF (Frump et al., 2021). A previous study from our group has

demonstrated that male Fischer CDF rats develop mal-adaptive RV remodeling in the SuHx model of PH compared to SD rats (Suen et al., 2019). The increased susceptibility to RHF in Fischer CDF rats was associated with lower angiogenic gene expression and lower vascular density and volume in these rats compared to SD rats. Similarly, in the present study, the adaptive RV remodeling in female rats was associated with a global increase in expression of angiogenic genes in the female RV compared to male RV. Surprisingly, these observations were not consistent with the density of EC as assessed by quantifying vWF expressing cells in the RV. While the vascular density and volume in our previous study were assessed using CD31 staining and fluorescence micro-angiography, respectively, in the present study we assessed EC density by vWF staining. Indeed, vWF staining in the heart has limitation including very low expression in cardiac microvascular EC (Yamamoto et al., 1998). Therefore, further assessment of vascular density using CD31 and wheat germ agglutinin, to measure microvascular density relative to cardiomyocyte, is needed. Overall, our data demonstrated up-regulation of angiogenic genes in the RV of female rats that demonstrated adaptive remodeling and further studies are needed to confirm differences in vascular density and underlying mechanisms.

Estradiol has been suggested to be pro-angiogenic and vascular protective in nature. Various studies have demonstrated that estradiol stimulates endothelial cell proliferation *in vitro* and *in vivo* (Concina et al., 2000; Krasinski et al., 1997; J. Liu et al., 2002; Morales et al., 1995; Reynolds et al., 1992). As well it has been associated with angiogenesis in the uterus and during tumor progression. Importantly, estradiol promotes angiogenic properties of isolated cardiac microvascular endothelial cells (H. Liu et al., 2018); however, the mechanisms remain unclear. Importantly, pro-angiogenic effects of estradiol on HUVEC are mediated by SPHK1 (Sukocheva et al., 2015) and our data demonstrated that female Fischer CDF rats subjected to PAB have higher relative expression of known angiogenic genes including SPHK1 in the RV. Therefore, we assessed expression of SPHK1 in the RVEC treated with estradiol. Our investigation showed that male RVECs in culture did not upregulate SPHK1 and CTGF; TGFβ2 was downregulated in response to estradiol at the 12 hr timepoint. These results are in line with the angiogenic gene array showing lower SPHK1 expression in male PAB rat RV relative to the female rats.

Additionally, estradiol treatment on male RVECs increased early network development. This suggests that estradiol stimulates blood vessel formation and these effects are independent of SPHK1 expression. Importantly, previous study demonstrated estradiol activated SPHK1 within 30 min suggesting that angiogenic effects of estradiol may involve direct activation of SPHK1. Further studies investigating the effect of estradiol on expression and activity of SPHK1 in male and female RVEC are needed to decipher the exact mechanisms by which estradiol promotes angiogenesis in male and female RVEC and their relevance to sex differences in RV adaptation.

4.2 Limitations

PAB is a very good model to study RV remodeling because of its specific and targeted effect in the RV and it is an excellent model for examining RV remodeling independent of other comorbidities and biological confounds (Evgenov et al., 2013). However, this also means that there is no clinical model or disease that resembles PAB and results cannot be generalized to clinical pathology (Evgenov et al., 2013). It is important to note that PAB model is not a progressive model and the RV afterload increases rapidly and remains constant. This may produce differences in RV remodeling compared to progressive models such as SuHx and MCT. These studies need to be repeated in SuHx model to better understand the sex differences in RV remodeling in RHF susceptible rat strain.

Results from our second cohort of rats showed that the only sex difference observed 4-weeks post-PAB was body weight. This is inconsistent with our 2-week results. Notably, the first rat cohorts were 6-8 weeks old and the final cohort was 5-7 weeks old when the intervention was introduced. Rats are considered adult at 6 weeks old, and it is possible that juvenile and adult rats have different adaptive abilities that explain the lack of sex differences in the younger cohort. This would be consistent with the literature which has demonstrated that children and adults have differences in their adaptation to PAH (Schäfer et al., 2019). Specifically, hemodynamic disease progression in PAH is less consistent in children and they have better prognoses regarding RHF than adults (Barst et al., 2011; Schäfer et al., 2019). Additionally, research has shown that, while adult females are more

likely to develop PAH than adult males, children do not exhibit the same differences in prevalence between sexes (Takatsuki et al., 2022).

4.2 Future Directions

To investigate the role of sex in RHF, PAB should be extended to 4-, 6-, and 8- week timepoints and adult rats should be used. It is possible that juvenile and adult rats have different adaptive abilities. These timepoints will allow researchers to examine the progression towards RHF and possible sex differences within animals. To further examine the role of sex, OVX and castrated animals should be included in these experiments and estradiol, progesterone, and testosterone can be independently supplemented. Supplementation conditions would provide valuable information about the role of each hormone. To address the limitations of the PAB model, future research should also examine RV failure in a model that more similarly represents natural pathology, like PH. The SuHx model is a strong method for developing PH and can be used to mitigate this limitation (Evgenov et al., 2013; Suen et al., 2019).

Future histological work should investigate other endothelial cell markers including PECAM and changes at later timepoints. This can be done using a method that allows for investigation of cardiomyocyte CSA and endothelial cell markers in the same tissue, such as wheat germ agglutinin. Using this method, slides could be stained with fluorescent agents targeting endothelial cells and cardiomyocytes.

mRNA and Matrigel experiments should also be repeated using primary female RVECs and compared to male RVEC to further examine the role of sex in pro-angiogenic gene expression and network forming ability. Furthermore, researchers should examine the density of estrogen and progesterone receptors in these cells using RT-qPCR or Western Blots. Variation in receptor density may influence hormone effect and response.

4.4 Conclusion

In conclusion, we demonstrated that there are significant sex differences in the expression of known angiogenic genes in response to PAB and adaption to increased afterload up to

the 2-week timepoint. Further research is needed to understand possible sex differences in longer term adaptations to increased afterload and to elucidate the mechanisms responsible for the observed sex differences.

BIBLIOGRAPHY

Antunes, M. J., Rodríguez-Palomares, J., Prendergast, B., De Bonis, M., Rosenhek, R., Al-Attar, N., Barili, F., Casselman, F., Folliguet, T., Iung, B., Lancellotti, P., Muneretto, C., Obadia, J.-F., Pierard, L., Suwalski, P., Zamorano, P., & on behalf of the ESC Working Groups of Cardiovascular Surgery and Valvular Heart Disease. (2017). Management of tricuspid valve regurgitation. *European Journal of Cardio-Thoracic Surgery*, *52*(6), 1022–1030. https://doi.org/10.1093/ejcts/ezx279

Aoki, M., Aoki, H., Mukhopadhyay, P., Tsuge, T., Yamamoto, H., Matsumoto, N. M., Toyohara, E., Okubo, Y., Ogawa, R., & Takabe, K. (2019). Sphingosine-1-Phosphate Facilitates Skin Wound Healing by Increasing Angiogenesis and Inflammatory Cell Recruitment with Less Scar Formation. *International Journal of Molecular Sciences*, *20*(14), 3381. https://doi.org/10.3390/ijms20143381

Arnal, J.-F., Fontaine, C., Billon-Galés, A., Favre, J., Laurell, H., Lenfant, F., & Gourdy, P. (2010). Estrogen Receptors and Endothelium. *Arteriosclerosis, Thrombosis, and Vascular Biology*, *30*(8), 1506–1512. https://doi.org/10.1161/ATVBAHA.109.191221

Barst, R. J., Ertel, S. I., Beghetti, M., & Ivy, D. D. (2011). Pulmonary arterial hypertension: A comparison between children and adults. *European Respiratory Journal*, *37*(3), 665–677. https://doi.org/10.1183/09031936.00056110

Beghetti, M., & Galiè, N. (2009). Eisenmenger Syndrome. *Journal of the American College of Cardiology*, *53*(9), 733–740. https://doi.org/10.1016/j.jacc.2008.11.025

Brida, M., Diller, G.-P., & Gatzoulis, M. A. (2018). Systemic Right Ventricle in Adults With Congenital Heart Disease: Anatomic and Phenotypic Spectrum and Current Approach to Management. *Circulation*, *137*(5), 508–518. https://doi.org/10.1161/CIRCULATIONAHA.117.031544

Burke, M. A., Katz, D. H., Beussink, L., Selvaraj, S., Gupta, D. K., Fox, J., Chakrabarti, S., Sauer, A. J., Rich, J. D., Freed, B. H., & Shah, S. J. (2014). Prognostic importance of pathophysiologic markers in patients with heart failure and preserved ejection fraction. *Circulation. Heart Failure*, *7*(2), 288–299. https://doi.org/10.1161/CIRCHEARTFAILURE.113.000854

Carabello, B. A. (2002). Concentric versus eccentric remodeling. *Journal of Cardiac Failure*, *8*(6), S258–S263. https://doi.org/10.1054/jcaf.2002.129250

Cassin, S., Dawes, G. S., Mott, J. C., Ross, B. B., & Strang, L. B. (1964). The Vascular Resistance Of The Foetal And Newly Ventilated Lung Of The Lamb. *The Journal of Physiology*, *171*, 61–79. https://doi.org/10.1113/jphysiol.1964.sp007361

Chia, E.-M., Hsieh, C. HC., Boyd, A., Pham, P., Vidaic, J., Leung, D., & Thomas, L. (2014). Effects of Age and Gender on Right Ventricular Systolic and Diastolic Function Using Two-Dimensional Speckle-Tracking Strain. *Journal of the American Society of Echocardiography*, *27*(10), 1079-1086.e1. https://doi.org/10.1016/j.echo.2014.06.007

Concina, P., Sordello, S., Barbacanne, M. A., Elhage, R., Pieraggi, M. T., Fournial, G., Plouet, J., Bayard, F., & Arnal, J. F. (2000). The mitogenic effect of 17beta-estradiol on in vitro endothelial cell proliferation and on in vivo reendothelialization are both dependent on vascular endothelial growth factor. *Journal of Vascular Research*, *37*(3), 202–208. https://doi.org/10.1159/000025732

Duca, F., Zotter-Tufaro, C., Kammerlander, A. A., Aschauer, S., Binder, C., Mascherbauer, J., & Bonderman, D. (2018). Gender-related differences in heart failure with preserved ejection fraction. *Scientific Reports*, *8*(1), 1080. https://doi.org/10.1038/s41598-018-19507-7

Evgenov, O. V., Humbert, M., & Stasch, J.-P. (Eds.). (2013). *Pharmacotherapy of Pulmonary Hypertension* (1st ed. 2013). Springer Berlin Heidelberg : Imprint: Springer. https://doi.org/10.1007/978-3-642-38664-0

Foderaro, A., & Ventetuolo, C. E. (2016). Pulmonary Arterial Hypertension and the Sex Hormone Paradox. *Current Hypertension Reports*, *18*(11), 84. https://doi.org/10.1007/s11906-016-0689-7

Friehs, I., Margossian, R. E., Moran, A. M., Cao-Danh, H., Moses, M. A., & Nido, P. J. (2006). Vascular endothelial growth factor delays onset of failure in pressure–overload hypertrophy through matrix metalloproteinase activation and angiogenesis. *Basic Research in Cardiology*, *101*(3), 204–213. https://doi.org/10.1007/s00395-005-0581-0

Frump, A. L., Albrecht, M., Yakubov, B., Breuils-Bonnet, S., Nadeau, V., Tremblay, E., Potus, F., Omura, J., Cook, T., Fisher, A., Rodriguez, B., Brown, R. D., Stenmark, K. R., Rubinstein, C. D., Krentz, K., Tabima, D. M., Li, R., Sun, X., Chesler, N. C., … Lahm, T. (2021). 17β-estradiol and estrogen receptor α protect right ventricular function in pulmonary hypertension via BMPR2 and apelin. *Journal of Clinical Investigation*, *131*(6), e129433. https://doi.org/10.1172/JCI129433

Frump, A. L., Bonnet, S., de Jesus Perez, V. A., & Lahm, T. (2018). Emerging role of angiogenesis in adaptive and maladaptive right ventricular remodeling in pulmonary hypertension. *American Journal of Physiology-Lung Cellular and Molecular Physiology*, *314*(3), L443–L460. https://doi.org/10.1152/ajplung.00374.2017. Copyright @ 2022 the American Physiological Society.

Frump, A. L., Goss, K. N., Vayl, A., Albrecht, M., Fisher, A., Tursunova, R., Fierst, J., Whitson, J., Cucci, A. R., Brown, M. B., & Lahm, T. (2015). Estradiol improves right ventricular function in rats with severe angioproliferative pulmonary hypertension: Effects of endogenous and exogenous sex hormones. *American Journal of Physiology-Lung Cellular and Molecular Physiology*, *308*(9), L873–L890. https://doi.org/10.1152/ajplung.00006.2015

Garvin, S., Nilsson, U. W., & Dabrosin, C. (2005). Effects of oestradiol and tamoxifen on VEGF, soluble VEGFR-1, and VEGFR-2 in breast cancer and endothelial cells. *British Journal of Cancer*, *93*(9), 1005–1010. https://doi.org/10.1038/sj.bjc.6602824

Giordano, F. J., Gerber, H.-P., Williams, S.-P., VanBruggen, N., Bunting, S., Ruiz-Lozano, P., Gu, Y., Nath, A. K., Huang, Y., Hickey, R., Dalton, N., Peterson, K. L., Ross, J., Chien, K. R., & Ferrara, N. (2001). A cardiac myocyte vascular endothelial growth factor paracrine pathway is required to maintain cardiac function. *Proceedings of the National Academy of Sciences*, *98*(10), 5780–5785. https://doi.org/10.1073/pnas.091415198

Gogiraju, R., Bochenek, M. L., & Schäfer, K. (2019). Angiogenic Endothelial Cell Signaling in Cardiac Hypertrophy and Heart Failure. *Frontiers in Cardiovascular Medicine*, *6*, 20. https://doi.org/10.3389/fcvm.2019.00020

Gomez-Arroyo, J. G., Farkas, L., Alhussaini, A. A., Farkas, D., Kraskauskas, D., Voelkel, N. F., & Bogaard, H. J. (2012). The monocrotaline model of pulmonary hypertension in perspective. *American Journal of Physiology-Lung Cellular and Molecular Physiology*, *302*(4), L363–L369. https://doi.org/10.1152/ajplung.00212.2011

Goumans, M.-J., Lebrin, F., & Valdimarsdottir, G. (2003). Controlling the Angiogenic SwitchA Balance between Two Distinct TGF-b Receptor Signaling Pathways. *Trends in Cardiovascular Medicine*, *13*(7), 301–307. https://doi.org/10.1016/S1050-1738(03)00142-7

Goumans, M.-J., Liu, Z., & ten Dijke, P. (2009). TGF-β signaling in vascular biology and dysfunction. *Cell Research*, *19*(1), 116–127. https://doi.org/10.1038/cr.2008.326

Grossman, W., & Paulus, W. J. (2013). Myocardial stress and hypertrophy: A complex interface between biophysics and cardiac remodeling. *Journal of Clinical Investigation*, *123*(9), 3701–3703. https://doi.org/10.1172/JCI69830

Hemnes, A. R., Maynard, K. B., Champion, H. C., Gleaves, L., Penner, N., West, J., & Newman, J. H. (2012). Testosterone Negatively Regulates Right Ventricular Load Stress Responses in Mice. *Pulmonary Circulation*, *2*(3), 352–358. https://doi.org/10.4103/2045-8932.101647

Hester, J., Ventetuolo, C., & Lahm, T. (2019). Sex, Gender, and Sex Hormones in Pulmonary Hypertension and Right Ventricular Failure. In R. Terjung (Ed.), *Comprehensive Physiology* (1st ed., pp. 125–170). Wiley. https://doi.org/10.1002/cphy.c190011

Heymans, S., González, A., Pizard, A., Papageorgiou, A. P., López-Andrés, N., Jaisser, F., Thum, T., Zannad, F., & Díez, J. (2015). Searching for new mechanisms of myocardial fibrosis with diagnostic and/or therapeutic potential: New mechanisms of myocardial fibrosis with diagnostic and/or therapeutic potential. *European Journal of Heart Failure*, *17*(8), 764–771. https://doi.org/10.1002/ejhf.312

Ho, S. Y., & Nihoyannopoulos, P. (2006). Anatomy, echocardiography, and normal right ventricular dimensions. *Heart (British Cardiac Society)*, *92 Suppl 1*, i2-13. https://doi.org/10.1136/hrt.2005.077875

Hoeper, M. M., Ghofrani, H.-A., Grünig, E., Klose, H., Olschewski, H., & Rosenkranz, S. (2017). Pulmonary Hypertension. *Deutsches Arzteblatt International*, *114*(5), 73–84. https://doi.org/10.3238/arztebl.2017.0073

Jain, V., Bordes, S. J., & Bhardwaj, A. (2022). Physiology, Pulmonary Circulatory System. In *StatPearls*. StatPearls Publishing. http://www.ncbi.nlm.nih.gov/books/NBK525948/

Jiang, B., Deng, Y., Suen, C., Taha, M., Chaudhary, K. R., Courtman, D. W., & Stewart, D. J. (2016). Marked Strain-Specific Differences in the SU5416 Rat Model of Severe Pulmonary Arterial Hypertension. *American Journal of Respiratory Cell and Molecular Biology*, *54*(4), 461–468. https://doi.org/10.1165/rcmb.2014-0488OC

Jozefczuk, E., Guzik, T. J., & Siedlinski, M. (2020). Significance of sphingosine-1-phosphate in cardiovascular physiology and pathology. *Pharmacological Research*, *156*, 104793. https://doi.org/10.1016/j.phrs.2020.104793

Kawel-Boehm, N., Maceira, A., Valsangiacomo-Buechel, E. R., Vogel-Claussen, J., Turkbey, E. B., Williams, R., Plein, S., Tee, M., Eng, J., & Bluemke, D. A. (2015). Normal values for cardiovascular magnetic resonance in adults and children. *Journal of Cardiovascular Magnetic Resonance*, *17*(1), 29. https://doi.org/10.1186/s12968-015-0111-7

Kawut, S. M., Lima, J. A. C., Barr, R. G., Chahal, H., Jain, A., Tandri, H., Praestgaard, A., Bagiella, E., Kizer, J. R., Johnson, W. C., Kronmal, R. A., & Bluemke, D. A. (2011). Sex and Race Differences in Right Ventricular Structure and Function: The Multi-Ethnic Study of Atherosclerosis–Right Ventricle Study. *Circulation*, *123*(22), 2542–2551. https://doi.org/10.1161/CIRCULATIONAHA.110.985515

Konstam, M. A., Kiernan, M. S., Bernstein, D., Bozkurt, B., Jacob, M., Kapur, N. K., Kociol, R. D., Lewis, E. F., Mehra, M. R., Pagani, F. D., Raval, A. N., & Ward, C. (2018). Evaluation and Management of Right-Sided Heart Failure: A Scientific Statement From the American Heart Association. *Circulation*, *137*(20). https://doi.org/10.1161/CIR.0000000000000560

Krasinski, K., Spyridopoulos, I., Asahara, T., van der Zee, R., Isner, J. M., & Losordo, D. W. (1997). Estradiol accelerates functional endothelial recovery after arterial injury. *Circulation*, *95*(7), 1768–1772. https://doi.org/10.1161/01.cir.95.7.1768

Kuang, D., Lei, Y., Yang, L., & Wang, Y. (2020). Preclinical study of a self-expanding pulmonary valve for the treatment of pulmonary valve disease. *Regenerative Biomaterials*, *7*(6), 609–618. https://doi.org/10.1093/rb/rbaa035

Kukulski, T., Hübbert, L., Arnold, M., Wranne, B., Hatle, L., & Sutherland, G. R. (2000). Normal Regional Right Ventricular Function and Its Change with Age: A Doppler Myocardial Imaging Study. *Journal of the American Society of Echocardiography*, *13*(3), 194–204. https://doi.org/10.1067/mje.2000.103106

Lai, K.-B., Sanderson, J. E., & Yu, C.-M. (2013). The regulatory effect of norepinephrine on connective tissue growth factor (CTGF) and vascular endothelial growth factor (VEGF) expression in cultured cardiac fibroblasts. *International Journal of Cardiology*, *163*(2), 183–189. https://doi.org/10.1016/j.ijcard.2011.06.003

Lakatos, B. K., Nabeshima, Y., Tokodi, M., Nagata, Y., Tősér, Z., Otani, K., Kitano, T., Fábián, A., Ujvári, A., Boros, A. M., Merkely, B., Kovács, A., & Takeuchi, M. (2020). Importance of Nonlongitudinal Motion Components in Right Ventricular Function: Three-Dimensional Echocardiographic Study in Healthy Volunteers. *Journal of the American Society of Echocardiography*, *33*(8), 995-1005.e1. https://doi.org/10.1016/j.echo.2020.04.002

Lewis, G. D., & Houstis, N. E. (2019). The Upsurge in Exercise Hemodynamic Measurements in Heart Failure With Preserved Ejection Fraction. *JACC: Heart Failure*, *7*(4), 333–335. https://doi.org/10.1016/j.jchf.2019.02.003

Liu, A., Philip, J., Vinnakota, K. C., Van den Bergh, F., Tabima, D. M., Hacker, T., Beard, D. A., & Chesler, N. C. (2017). Estrogen maintains mitochondrial content and function in the right ventricle of rats with pulmonary hypertension. *Physiological Reports*, *5*(6), e13157. https://doi.org/10.14814/phy2.13157

Liu, H., Tao, Y., Chen, M., Yu, J., Li, W.-J., Tao, L., Li, Y., & Li, F. (2018). 17β-Estradiol Promotes Angiogenesis of Rat Cardiac Microvascular Endothelial Cells In Vitro. *Medical Science Monitor: International Medical Journal of Experimental and Clinical Research*, *24*, 2489–2496. https://doi.org/10.12659/msm.903344

Liu, J., Wu, S., Wei, H., Zhou, K., Ruan, Y., & Lai, W. (2002). Effects of sex hormones and their balance on the proliferation of rat vascular endothelial cells. *Hormone Research*, *58*(1), 16–20. https://doi.org/10.1159/000063211

Losordo, D. W., & Isner, J. M. (2001). Estrogen and Angiogenesis: A Review. *Arteriosclerosis, Thrombosis, and Vascular Biology*, *21*(1), 6–12. https://doi.org/10.1161/01.ATV.21.1.6

Maganti, K., Rigolin, V. H., Sarano, M. E., & Bonow, R. O. (2010). Valvular heart disease: Diagnosis and management. *Mayo Clinic Proceedings*, *85*(5), 483–500. https://doi.org/10.4065/mcp.2009.0706

Mandras, S. A., & Desai, S. (2022). Right Heart Failure. In *StatPearls*. StatPearls Publishing. http://www.ncbi.nlm.nih.gov/books/NBK459381/

McGoon, M. D., & Miller, D. P. (2012). REVEAL: A contemporary US pulmonary arterial hypertension registry. *European Respiratory Review*, *21*(123), 8–18. https://doi.org/10.1183/09059180.00008211

Means, C. K., & Brown, J. H. (2008). Sphingosine-1-phosphate receptor signalling in the heart. *Cardiovascular Research*, *82*(2), 193–200. https://doi.org/10.1093/cvr/cvp086

Minullina, I. R., Alexeyeva, N. P., Anisimov, S. V., Puzanov, M. V., Kozlova, S. N., Sviryaev, Y. V., Zaritskey, A. Y., & Shlyakhto, E. V. (2014). Transcriptional changes in bone marrow stromal cells of patients with heart failure. *Cell Cycle*, *13*(9), 1495–1500. https://doi.org/10.4161/cc.28472

Moon, S., Lee, S., Caesar, J. A., Pruchenko, S., Leask, A., Knowles, J. A., Sinon, J., & Chaqour, B. (2020). A CTGF-YAP Regulatory Pathway Is Essential for Angiogenesis and Barriergenesis in the Retina. *IScience*, *23*(6), 101184. https://doi.org/10.1016/j.isci.2020.101184

Morales, D. E., McGowan, K. A., Grant, D. S., Maheshwari, S., Bhartiya, D., Cid, M. C., Kleinman, H. K., & Schnaper, H. W. (1995). Estrogen promotes angiogenic activity in human umbilical vein endothelial cells in vitro and in a murine model. *Circulation*, *91*(3), 755–763. https://doi.org/10.1161/01.cir.91.3.755

Pengo, V., Lensing, A. W. A., Prins, M. H., Marchiori, A., Davidson, B. L., Tiozzo, F., Albanese, P., Biasiolo, A., Pegoraro, C., Iliceto, S., & Prandoni, P. (2004). Incidence of Chronic Thromboembolic Pulmonary Hypertension after Pulmonary Embolism. *New England Journal of Medicine*, *350*(22), 2257–2264. https://doi.org/10.1056/NEJMoa032274

Piao, L., Marsboom, G., & Archer, S. L. (2010). Mitochondrial metabolic adaptation in right ventricular hypertrophy and failure. *Journal of Molecular Medicine*, *88*(10), 1011–1020. https://doi.org/10.1007/s00109-010-0679-1

Pignatelli, R. H., Noel, C., & Reddy, S. C. B. (2017). Imaging of the pulmonary valve in the adults. *Current Opinion in Cardiology*, *32*(5), 529–540. https://doi.org/10.1097/HCO.0000000000000436

Pinto, A. R., Ilinykh, A., Ivey, M. J., Kuwabara, J. T., D'Antoni, M. L., Debuque, R., Chandran, A., Wang, L., Arora, K., Rosenthal, N. A., & Tallquist, M. D. (2016). Revisiting Cardiac Cellular Composition. *Circulation Research*, *118*(3), 400–409. https://doi.org/10.1161/CIRCRESAHA.115.307778

Pitoulis, F. G., & Terracciano, C. M. (2020). Heart Plasticity in Response to Pressure- and Volume-Overload: A Review of Findings in Compensated and Decompensated Phenotypes. *Frontiers in Physiology*, *11*, 92. https://doi.org/10.3389/fphys.2020.00092

Poch, D., & Mandel, J. (2021). Pulmonary Hypertension. *Annals of Internal Medicine*, *174*(4), ITC49–ITC64. https://doi.org/10.7326/AITC202104200

Potus, F., Ruffenach, G., Dahou, A., Thebault, C., Breuils-Bonnet, S., Tremblay, È., Nadeau, V., Paradis, R., Graydon, C., Wong, R., Johnson, I., Paulin, R., Lajoie, A. C., Perron, J., Charbonneau, E., Joubert, P., Pibarot, P., Michelakis, E. D., Provencher, S., & Bonnet, S. (2015). Downregulation of MicroRNA-126 Contributes to the Failing Right Ventricle in Pulmonary Arterial Hypertension. *Circulation*, *132*(10), 932–943. https://doi.org/10.1161/CIRCULATIONAHA.115.016382

Prins, K. W., & Thenappan, T. (2016). World Health Organization Group I Pulmonary Hypertension: Epidemiology and Pathophysiology. *Cardiology Clinics*, *34*(3), 363–374. https://doi.org/10.1016/j.ccl.2016.04.001

Prisco, S. Z., Thenappan, T., & Prins, K. W. (2020). Treatment Targets for Right Ventricular Dysfunction in Pulmonary Arterial Hypertension. *JACC: Basic to Translational Science*, *5*(12), 1244–1260. https://doi.org/10.1016/j.jacbts.2020.07.011

Reynolds, L. P., Killilea, S. D., & Redmer, D. A. (1992). Angiogenesis in the female reproductive system. *FASEB Journal: Official Publication of the Federation of American Societies for Experimental Biology*, *6*(3), 886–892.

Ribatti, D. (2013). Angiogenesis. In *Brenner's Encyclopedia of Genetics* (pp. 130–132). Elsevier. https://doi.org/10.1016/B978-0-12-374984-0.00065-6

Sahay, S. (2019). Evaluation and classification of pulmonary arterial hypertension. *Journal of Thoracic Disease*, *11*(Suppl 14), S1789–S1799. https://doi.org/10.21037/jtd.2019.08.54

Sanz, J., Sánchez-Quintana, D., Bossone, E., Bogaard, H. J., & Naeije, R. (2019). Anatomy, Function, and Dysfunction of the Right Ventricle: JACC State-of-the-Art Review. *Journal of the American College of Cardiology*, *73*(12), 1463–1482. https://doi.org/10.1016/j.jacc.2018.12.076

Schäfer, M., Ivy, D. D., Abman, S. H., Stenmark, K., Browne, L. P., Barker, A. J., Mitchell, M. B., Morgan, G. J., Wilson, N., Shah, A., Kollengode, M., Naresh, N., Fonseca, B., DiMaria, M., Buckner, J. K., Hunter, K. S., Kheyfets, V., Fenster, B. E., & Truong, U. (2019). Differences in pulmonary arterial flow hemodynamics between children and adults with pulmonary arterial hypertension as assessed by 4D-flow CMR studies. *American Journal of Physiology-Heart and Circulatory Physiology*, *316*(5), H1091–H1104. https://doi.org/10.1152/ajpheart.00802.2018

Schimmel, K., Ichimura, K., Reddy, S., Haddad, F., & Spiekerkoetter, E. (2022). Cardiac Fibrosis in the Pressure Overloaded Left and Right Ventricle as a Therapeutic Target. *Frontiers in Cardiovascular Medicine*, *9*, 886553. https://doi.org/10.3389/fcvm.2022.886553

Siedlinski, M., Nosalski, R., Szczepaniak, P., Ludwig-Gałęzowska, A. H., Mikołajczyk, T., Filip, M., Osmenda, G., Wilk, G., Nowak, M., Wołkow, P., & Guzik, T. J. (2017). Vascular transcriptome profiling identifies Sphingosine kinase 1 as a modulator of angiotensin II-induced vascular dysfunction. *Scientific Reports*, *7*(1), 44131. https://doi.org/10.1038/srep44131

Sim, C. B., Phipson, B., Ziemann, M., Rafehi, H., Mills, R. J., Watt, K. I., Abu-Bonsrah, K. D., Kalathur, R. K. R., Voges, H. K., Dinh, D. T., Ter Huurne, M., Vivien, C. J., Kaspi, A., Kaipananickal, H., Hidalgo, A., Delbridge, L. M. D., Robker, R. L., Gregorevic, P., Dos Remedios, C. G., … Porrello, E. R. (2021). Sex-Specific Control of Human Heart Maturation by the Progesterone Receptor. *Circulation*, *143*(16), 1614–1628. https://doi.org/10.1161/CIRCULATIONAHA.120.051921

St. Pierre, S. R., Peirlinck, M., & Kuhl, E. (2022). Sex Matters: A Comprehensive Comparison of Female and Male Hearts. *Frontiers in Physiology*, *13*, 831179. https://doi.org/10.3389/fphys.2022.831179

Suen, C. M., Chaudhary, K. R., Deng, Y., Jiang, B., & Stewart, D. J. (2019). Fischer rats exhibit maladaptive structural and molecular right ventricular remodelling in severe pulmonary hypertension: A genetically prone model for right heart failure. *Cardiovascular Research*, *115*(4), 788–799. https://doi.org/10.1093/cvr/cvy258

Sukocheva, O., Wadham, C., Gamble, J., & Xia, P. (2015). Sphingosine-1-phosphate receptor 1 transmits estrogens' effects in endothelial cells. *Steroids*, *104*, 237–245. https://doi.org/10.1016/j.steroids.2015.10.009

Sun, X.-Q., Abbate, A., & Bogaard, H.-J. (2017). Role of cardiac inflammation in right ventricular failure. *Cardiovascular Research*, *113*(12), 1441–1452. https://doi.org/10.1093/cvr/cvx159

Swift, A. J., Capener, D., Hammerton, C., Thomas, S. M., Elliot, C., Condliffe, R., Wild, J. M., & Kiely, D. G. (2015). Right Ventricular Sex Differences in Patients with Idiopathic Pulmonary Arterial Hypertension Characterised by Magnetic Resonance Imaging: Pair-Matched Case Controlled Study. *PLOS ONE*, *10*(5), e0127415. https://doi.org/10.1371/journal.pone.0127415

Takatsuki, S., Shimokawahara, H., Shimizu, Y., Kawai, R., Matsuura, H., & Matsubara, H. (2022). Clinical differences between children and adults with idiopathic and heritable pulmonary arterial hypertension. *Cardiology in the Young*, 1–4. https://doi.org/10.1017/S1047951122003432

ten Dijke, P., & Arthur, H. M. (2007). Extracellular control of TGFβ signalling in vascular development and disease. *Nature Reviews Molecular Cell Biology*, *8*(11), 857–869. https://doi.org/10.1038/nrm2262

Thandavarayan, R. A., Chitturi, K. R., & Guha, A. (2020). Pathophysiology of Acute and Chronic Right Heart Failure. *Cardiology Clinics*, *38*(2), 149–160. https://doi.org/10.1016/j.ccl.2020.01.009

Trenti, A., Tedesco, S., Boscaro, C., Trevisi, L., Bolego, C., & Cignarella, A. (2018). Estrogen, Angiogenesis, Immunity and Cell Metabolism: Solving the Puzzle. *International Journal of Molecular Sciences*, *19*(3), 859. https://doi.org/10.3390/ijms19030859

Tretter, J. T., & Redington, A. N. (2018). The Forgotten Ventricle?: The Left Ventricle in Right-Sided Congenital Heart Disease. *Circulation: Cardiovascular Imaging*, *11*(3), e007410. https://doi.org/10.1161/CIRCIMAGING.117.007410

van Campen, J. S. J. A., de Boer, K., van de Veerdonk, M. C., van der Bruggen, C. E. E., Allaart, C. P., Raijmakers, P. G., Heymans, M. W., Marcus, J. T., Harms, H. J., Handoko, M. L., de Man, F. S., Vonk Noordegraaf, A., & Bogaard, H.-J. (2016). Bisoprolol in idiopathic pulmonary arterial hypertension: An explorative study. *European Respiratory Journal*, *48*(3), 787–796. https://doi.org/10.1183/13993003.00090-2016

van de Veerdonk, M. C., Bogaard, H. J., & Voelkel, N. F. (2016). The right ventricle and pulmonary hypertension. *Heart Failure Reviews*, *21*(3), 259–271. https://doi.org/10.1007/s10741-016-9526-y

van de Veerdonk, M. C., Kind, T., Marcus, J. T., Mauritz, G.-J., Heymans, M. W., Bogaard, H.-J., Boonstra, A., Marques, K. M. J., Westerhof, N., & Vonk-Noordegraaf, A. (2011). Progressive right ventricular dysfunction in patients with pulmonary arterial hypertension responding to therapy. *Journal of the American College of Cardiology*, *58*(24), 2511–2519. https://doi.org/10.1016/j.jacc.2011.06.068

Ventetuolo, C. E., Ouyang, P., Bluemke, D. A., Tandri, H., Barr, R. G., Bagiella, E., Cappola, A. R., Bristow, M. R., Johnson, C., Kronmal, R. A., Kizer, J. R., Lima, J. A. C., & Kawut, S. M. (2011). Sex hormones are associated with right ventricular structure and function: The MESA-right ventricle study. *American Journal of Respiratory and Critical Care Medicine*, *183*(5), 659–667. https://doi.org/10.1164/rccm.201007-1027OC

Voelkel, N. F., Quaife, R. A., Leinwand, L. A., Barst, R. J., McGoon, M. D., Meldrum, D. R., Dupuis, J., Long, C. S., Rubin, L. J., Smart, F. W., Suzuki, Y. J., Gladwin, M., Denholm, E. M., & Gail, D. B. (2006). Right Ventricular Function and Failure: Report of a National Heart, Lung, and Blood Institute Working Group on Cellular and Molecular Mechanisms of Right Heart Failure. *Circulation*, *114*(17), 1883–1891. https://doi.org/10.1161/CIRCULATIONAHA.106.632208

Walker, L. A., & Buttrick, P. M. (2013). The right ventricle: Biologic insights and response to disease: updated. *Current Cardiology Reviews*, *9*(1), 73–81. https://doi.org/10.2174/157340313805076296

Wang, J. M. H., Rai, R., Carrasco, M., Sam-Odusina, T., Salandy, S., Gielecki, J., Zurada, A., & Loukas, M. (2019). An anatomical review of the right ventricle. *Translational Research in Anatomy*, *17*, 100049. https://doi.org/10.1016/j.tria.2019.100049

Wijeratne, D. T., Lajkosz, K., Brogly, S. B., Lougheed, M. D., Jiang, L., Housin, A., Barber, D., Johnson, A., Doliszny, K. M., & Archer, S. L. (2018). Increasing Incidence and Prevalence of World Health Organization Groups 1 to 4 Pulmonary Hypertension: A Population-Based Cohort Study in Ontario, Canada. *Circulation: Cardiovascular Quality and Outcomes*, *11*(2), e003973. https://doi.org/10.1161/CIRCOUTCOMES.117.003973

Xiong, Y., & Hla, T. (2014). S1P Control of Endothelial Integrity. In M. B. A. Oldstone & H. Rosen (Eds.), *Sphingosine-1-Phosphate Signaling in Immunology and Infectious Diseases* (Vol. 378, pp. 85–105). Springer International Publishing. https://doi.org/10.1007/978-3-319-05879-5_4

Yamamoto, K., de Waard, V., Fearns, C., & Loskutoff, D. J. (1998). Tissue distribution and regulation of murine von Willebrand factor gene expression in vivo. *Blood*, *92*(8), 2791–2801.

Yancopoulos, G. D., Davis, S., Gale, N. W., Rudge, J. S., Wiegand, S. J., & Holash, J. (2000). Vascular-specific growth factors and blood vessel formation. *Nature*, *407*(6801), 242–248. https://doi.org/10.1038/35025215

Yoo, B. W. (2018). Epidemiology of Congenital Heart Disease with Emphasis on Sex-Related Aspects. In P. L. M. Kerkhof & V. M. Miller (Eds.), *Sex-Specific Analysis of Cardiovascular Function* (Vol. 1065, pp. 49–59). Springer International Publishing. https://doi.org/10.1007/978-3-319-77932-4_3

Zaffran, S., Kelly, R. G., Meilhac, S. M., Buckingham, M. E., & Brown, N. A. (2004). Right Ventricular Myocardium Derives From the Anterior Heart Field. *Circulation Research*, *95*(3), 261–268. https://doi.org/10.1161/01.RES.0000136815.73623.BE

Zelt, J. G. E., Chaudhary, K. R., Cadete, V. J., Mielniczuk, L. M., & Stewart, D. J. (2019). Medical Therapy for Heart Failure Associated With Pulmonary Hypertension. *Circulation Research*, *124*(11), 1551–1567. https://doi.org/10.1161/CIRCRESAHA.118.313650

Zhang, Q., Wang, L., Wang, S., Cheng, H., Xu, L., Pei, G., Wang, Y., Fu, C., Jiang, Y., He, C., & Wei, Q. (2022). Signaling pathways and targeted therapy for myocardial infarction. *Signal Transduction and Targeted Therapy*, *7*(1), 78. https://doi.org/10.1038/s41392-022-00925-z